BACHELOR'S THESIS / BIOMEDICAL ENGINEERING 2021

Development of an open-source, wireless and implantable vagus nerve stimulator for preclinical studies in mice.

Marcos Chic Cóbreces

upf. Universitat Pompeu Fabra Barcelona

Development of an open-source, wireless and implantable vagus nerve stimulator for preclinical studies in mice.

Marcos Chic Cóbreces

Bachelor's thesis UPF 2020/2021

Thesis supervisor(s):

Dr. Antoni Ivorra

Dr. Laura Becerra-Fajardo

Dedicatory

Por Judith y Elías.
A Jesús y Chon.

Acknowledgments

To my two supervisors for their advice, their trust and their patience. Also, to the rest of the team members of the Biomedical Electronics Research Group for their kindness and their help (Aracelys, Jaume...). Finally, to the Pompeu Fabra University for the opportunity.

Abstract

The advantages of electrical neuromodulation-based treatments over pharmacological and surgical approaches are clear since they mean a non destructive and reversible alternative. Moreover, they can avoid the large ingest of drugs that many treatments entail nowadays, avoiding therefore their side effects. Vagus nerve stimulation is expected to be a promising neuromodulation therapy capable of treating a wide variety of diseases like obesity, atherosclerosis, type II diabetes or heart failure; moreover it has already been approved for depression and epilepsy. Vagus nerve (tenth cranial nerve) constitutes an interesting target for this type of stimulation since it is well known that it plays a major role in inflammatory pathways and the amount of diseases related with inflammations is huge (e.g. inflammatory bowel disease, rheumatoiod arthritis etc.). Taking all of this into consideration, it can be understood the increasing need of functional long-lasting vagus nerve stimulators for pre-clinical research in rodent models. In addition, the current lack of this type of commercial stimulators (none of them open-source) in the market makes this work more essential. As a first step of a series of bachelor thesis (BT), this BT proposes the development of a device aimed to be open-source and fully implantable and wireless, avoiding thus percutaneous wiring that makes the stimulator less hardwearing. To accomplish this, it has been proposed a small device (10 mm of diameter) based only on commercially available components and powered by a 3V coin battery. Besides, it is current controlled and delivers passive biphasic pulses for the stimulation. This device is part of a whole vagus nerve stimulation system, which would also include the cuff electrodes (whose design and manufacture has also been developed in this BT) and the encapsulation.

Keywords

Neurostimulation, vagus nerve, implantable, wireless, mice.

Prologue

As medicine and technology evolve, different alternatives to already-established treatments appear. In order to make that possible, preclinical studies play a crucial role. However, in many cases so that these studies can be carried out advances in technology are required. It is the case of vagus nerve electrical stimulation, which despite being a really suggestive potential therapy for different diseases, could be facing problems to perform chronic animal experiments due to the lack of implantable stimulators. Present work is a first step towards the development of a novel implantable, wireless and open-source vagus nerve stimulator for mice. Then, this bachelor thesis is expected to be followed by future BTs of other students, aiming to carry on the development of the device proposed here and therefore helping the scientific community involved in the research of the effects of vagus nerve stimulation.

Index

List of figures

List of tables

1. INTRODUCTION

1.1 Vagus nerve physiology

Vagus nerve, which used to be known as pneumogastric nerve, constitutes the tenth pair cranial nerve (CN X) and it is in fact the longest of them all. It makes part of the autonomic nervous system, which means that it regulates involuntary physiological processes [1]. Moreover, since it is a mixed nerve it performs two types of tasks; sensory and motor, being thus projected in the afferent (~80% of its fibres) and the efferent (~20% of its fibres) directions [2] These fibres are mainly of three different types: A-type fibres, B- type fibres and C-type fibres. While the first two groups are largely myelinated and have diameters of 5-20 μm and 1-3 μm respectively, C fibres tend to be finer (0.4-2 μm of diameter) and are not myelinated [3] [4]. Regarding the anatomy of the nerve, it originates in the medulla oblongata, a region of the brain mainly devoted to autonomic functions. From there, it travels bilaterally through the brainstem and starts branching and innervating several organs [1].

In spite of the fact that not all the innervations of the vagus nerve are known yet, they can be grouped in three main regions: neck, thorax and abdomen. The major organs of the thorax innervated by this nerve are the heart, the bronchi, the lungs and the esophagus [5] [6]. In the abdomen branches of the vagus nerve reach stomach, liver, pancreas, duodenum and some tracts of the colon [6]. As a consequence of heart efferent innervations, this nerve has an impact on cardiovascular parameters such as heart rate and blood pressure. However, while right vagus nerve is attached to the sinoatrial node (and therefore has more to do with the first parameter mentioned), left vagus nerve innervates the atrioventricular node (thus having more impact in the second parameter) [3]. Other efferent innervations that travel to the abdomen are considered to be crucial in reflex gastric accommodation and hence in ingest of meal by varying gastric tone [7]. Furthermore, vagus nerve activation triggers cholinergic anti-inflammatory pathways, leading to a decrease in TNF (tumour necrosis factor) in liver, spleen and heart. This way of suppressing inflammation by cholinergic pathways instead of by neural-based pathways offers some advantages, namely that it is discrete and more localized [8]. This generates a lot of interest due to the amount of chronic and autoimmune diseases associated with inflammation, for instance chronic obstructive pulmonary disease, asthma, allergies or multiple sclerosis [5]. In addition to this, there are many diseases that may be treated by all of the innervations that have been mentioned above. Here it should be distinguished between already approved therapies and potential ones. In the first group we can find depression and epilepsy. In the second group other diseases like obesity, cardiovascular disorders, diabetes, sepsis or traumatic brain injury (TBI) are being investigated [1] [3]. In the case of epilepsy, this type of treatment is frequently reserved for those patients who suffer from pharmacoresistance and it is applied through an implanted stimulator that delivers the pulses to the left cervical vagus [9]. However, it has to be stated that the way vagus nerve stimulation (VNS) stops epilepsy seizures remains unknown. Regarding depression, its treatment with VNS is approved since 2005, when the FDA allowed it but only for chronic or recurring cases [10]. For depression the mechanism of action is believed to influence in the medial and prefrontal cortex, where neurotransmitters associated with anti-depression effects (such as serotonin) are released [10]. When it comes to the diseases in which the treatment of VNS is still being investigated as an alternative, it can be found that, for example in obesity, studies in pigs have been carried out resulting in a decrease of weight due to a lowering in food intake [11]. Similar studies have been

performed by Zhang et al. [12], but in this case in order to research about how VNS improves heart function and in a canine model. Others like Meyers et al. [13] focused on diabetes type II, managing to decrease glucose levels in blood by selective efferent stimulation.

Nevertheless, some side effects when applying VNS have also been reported. For instance, in the treatment of epilepsy under the FDA-approved (Food and Drug Administration) conditions the most common ones have been cough, dysphonia and hoarseness [14]. However, these adverse effects were only present during the stimulation period and are related with the strength of the stimulation (current amplitude, frequency, duty cycle...). The appearance of bradycardia has also been reported as a possible side effect [15], but it is not clinically relevant if stimulation is performed in accordance with the FDA-approved guidelines for VNS [16].

1.2 Electrical stimulation

In addition to what has just been explained, in order to understand how VNS works some fundamentals about electrical stimulation of excitable tissue should be mentioned. First of all, when an electrode is introduced into the body to deliver pulses to a nerve two separated interfaces show up, one is the metal (called electrode) and the other one is the extracellular medium surrounding the metal (called electrolyte). In the electrode charge is carried by electrons, while in the electrolyte it is carried by ions. Therefore, when an electrical pulse is sent by setting a voltage difference between electrodes, electrons travel from one electrode to the other, thus generating an electrode with positive potential and an electrode with negative potential [17]. The one which has been driven negative is called cathode and starts attracting cations and repelling anions, therefore an electric field is generated into the electrolyte. The phenomenon that has just been explained is known as the charge and discharge of the double layer capacitance, which is generated in the electrode/electrolyte interface. However, this only occurs as long as the injected charge does not exceed a certain threshold, otherwise electron transfer between electrode-electrolyte happens, creating Faradaic reactions. This type of reactions can affect both cathode and anode. In the first case, stimulation can generate undesired products in the electrolyte that leave the interface and travel being potentially harmful for the tissue. In the second case, the surface of the anode can oxidise also releasing substances that can damage the medium [17]. All in all, it is this charge redistribution into the tissue what can provoke action potentials by increasing the probability of voltage-gated ion channels in the neurons to open. When this happens, current spreads from the node of Ranvier which is closest to the cathode to the surrounding nodes creating a wave [18].

This type of stimulation is mostly applied in two main regions; the ear where the auricula or the cymba conchae are the typical targets [19] [20], and the cervical region where two branches of the vagus nerve appear (i.e. left and right) [21]. In the first case stimulation is transcutaneous and in the second one the electrodes must be implanted. When it comes to cervical VNS stimulation, it does not have the same consequences delivering it in the right or in the left branch, since each one innervates different targets. These differences between the innervations of cervical branches were explained above and lead to a preponderance of left cervical VNS over right one in order to minimize risks.

1.3 Stimulation parameters

The proportion of types of fibres in the vagus nerve is also relevant to determine how the stimulation is carried out. The majority of the fibres seem to be C-type, ranging from 65% to 80% of the total composition and yielding 20-35% for A-type and B-type [4]. The current threshold needed to activate C-type fibres is over 2mA, while A-type fibres need currents ranging from 0.02 to 0.2mA and B-type fibres from 0.04 to 0.6 mA [3]. Therefore, if spiking of all the fibres aims to be provoked, stimulators should supply currents above 2mA. However, it has been proved that stimulation of C-fibres does not have clinical relevance (at least when it comes to epilepsy treatment) [22], and since such high currents increase the risk of suffering from side effects as it has been mentioned previously, they tend to be avoided. Another crucial parameter is the frequency of the stimulation, which also has a lot to do with the potential adverse effects. In this case, it has been proved that prolonged stimulation frequencies over 50Hz can lead to irreversible early axonal degeneration (EAD) [23]. This type of damage seems to be related with the hyperactivity of the fibres of the nerve, what leads to a collapse of the myelin into the axoplasm and to axonal degeneration due to the action of macrophages [24]. Thus, current stimulation frequencies go from 20Hz to 30Hz [25] [3]. With respect to the width of the pulses, this parameter is strongly correlated with the current amplitude since both parameters will determine the amount of delivered charge; this relationship is called strength-duration. The wider a pulse is, the less amplitude is needed in the pulse to elicit an action potential (this is threshold current decreases), because more charge is being injected. Therefore, the relation between threshold current and pulse duration tends asymptotically to a minimum value of threshold current which is known as rheobase current (I_r) [18]. However, the more a pulse lasts, the more charge is injected into the nerve, which increases the probability of leading to tissue damage. From this we can appreciate that the stimulation of excitable tissue is a trade-off between injecting enough charge to get action potentials but not too much so that injuries can be avoided. Taking this into consideration, common pulse widths in rodents for VNS are smaller than 1000μs [21]. Finally, the duty cycle of the stimulator in accordance with the FDA guidelines for the treatment of people with epilepsy is 30 s in ON state and 5 min in OFF state [21].

1.4 Stimulation configuration

Another important pillar in this field is the type of pulses that are used for the stimulation. In peripheral nerve stimulation the pulses applied are most commonly biphasic [26] [27] [28] [29] [21], this means that each cathodic pulse is followed by an anodic pulse. While the cathodic pulse depolarizes the tissue trying to give place to an action potential, anodic currents hyperpolarize. The aim of biphasic pulses is to minimize the production of Faradaic reactions that may result in undesired electrochemical process. For instance, the reduction of water generates products that can change the pH of a solution [30] [31] [32]. Something else that has to be taken into consideration is that depending on the potential that is being applied in biphasic stimulation, the anodic pulse can also lead to electrodes transfer from the electrolyte to the electrode. To avoid this issue, instead of applying a complete charge-balanced stimulation, charge imbalanced pulses are also used, that entails reducing the amplitude of the anodic phase [17] [33]. On the other hand, one of the disadvantages of a biphasic configuration is that unlike monophasic design (consisting in an only depolarizing wave), it implies more complex electronics and tends to use more volume, yielding therefore a device with a bigger volume (remind that miniaturization is one of the main challenges for implantable devices).

A big concern when it comes to the configuration of the stimulation is if it has to be either voltage-controlled or current-controlled. The first type of them refers to a design where the voltage is fixed during the whole process, this means that the current that is being applied in the stimulation depends on the resistance of the electrode (by Ohm's law). Therefore, if the impedance of the electrode changes due to some circumstance such as a partial detachment from the nerve, the delivered current will also change. This is what makes of voltage control a less precise and reproducible alternative. On the other side we have current control, where the system is designed so that the delivered current keeps fixed at certain amplitude. Thus, in this case, current is not a function of time since it does not depend on the impedance of the electrode. Despite both types of configuration can provoke action potentials and voltage control is simpler (because it does not require the feedback circuitry that is indispensable for current control) [18], the previously mentioned advantage makes current control more frequently used for the stimulation of excitable tissue [21] [29] [27] [34].

1.5 Stimulation electrodes

In order to deliver these stimulation pulses, electrodes are implanted around the nerve. Electrodes can be classified in two main groups, those ones which wrap around the nerve interfacing with lots of axons at the same time or intrafascicular electrodes, which penetrate the nerve and are in contact only with a small group of axons [35]. In that first group three types of them can be distinguished: hook, coil and cuff electrodes. Cuff electrodes are commonly preferred for nerve stimulation due to the fact that they offer some advantages over hook or coil electrodes [21]. First, the cuff helps to avoid detachments and drifts of the electrode from the surface of the nerve improving the contact interface. Such a fixed placement of the electrodes is more difficult to accomplish with coil or hook types and if the stimulator works in voltage control this can lead to problems as we have previously mentioned. Another benefit is that the cuff prevents current leaking out of the nerve, which could lead to undesired stimulation of neighbour nerves or injection of charge in surrounding tissues. This is not only an advantage due to the obvious point of the protection, but also because current leaks make that more current is needed to activate the target nerve increasing power consumption of the stimulator [35] [36].

1.6 Vagus nerve stimulation at Pompeu Fabra University

Regarding the framework of this project in our university, it is motivated by the work of the laboratory of Andrés Ozaita (Neuropharmacology Department Research Group), which is studying how connectivity between different brain regions is affected by VNS. To do so without working with anesthetized mice different alternatives have been proposed. One possibility is placing an Elizabethan collar around the neck of the mouse and making a hole in the collar. In this way, a wire with the electrodes could be passed through the collar in order to locate the electrodes in the surface of the ear, where VNS could take place. Elizabethan collar would not allow the mouse to pull out the electrodes from its ear with its paws. In this case, current would come from an external generator. Nevertheless, this alternative entails some major drawbacks. Firstly, it impossibilities chronic stimulation since the collar really limits the activity of the mouse. In addition to that, Elizabethan collar is annoying for the mouse, what can change its behaviour and disturb activities like grooming or establishing social relations with other rodents. Taking all this into account, an implantable vagus nerve stimulator

that delivers pulses in the cervical region of the nerve such as the one is aimed to be designed in this project could be an interesting option. By avoiding head-mounted devices or tethering, it would allow chronic stimulation and should not interfere in the common behaviour of the mouse once it is implanted.

1.7 Commercially-available stimulators

In fact, two commercial implantable devices for VNS in mice which would accomplish this function have been found. To get to know them better contact has been established with both fabricants. The first one of them is offered by Harald Strauss Scientific [37] [38] (although it is no longer distributed through this company but through the Burrell College of Osteopathic Medicine) (see *Fig. 1*). The other one is commercialised by Invilog Research Ltd (see *Fig. 2*). The first one is a rather rudimentary device which has around 15 mm of length and is connected to a couple of coil electrodes; the whole device weights 1.2g. Moreover, it can apply biphasic pulses of 3V as maximum with a maximum frequency of 5000Hz, while it is voltage-controlled. Six different configurations for the stimulation can be programmed in this device and the way to change between them is the same one that is used to switch on the stimulator, this is by using a magnetic switch. Its prize is 250$. On the other hand, when it comes to the stimulator of Invilog, it can be used for either rats or mice. The dimensions are a bit smaller since it has a diameter of 13 mm and a thickness of 3 mm, its weight is 1.4g. One of the biggest differences with respect to the previous stimulator is that this one uses current control, also noticeable is the fact that current pulses are monophasic here. A maximum voltage of 18V and maximum frequencies of 500Hz can be reached. Furthermore, it includes the possibility of changing the stimulation configuration and switching it ON or OFF remotely. Finally, this stimulator is sold in batches of six devices, what makes its purchase rather expensive (taking also into account that they do not include electrodes) since each one of them costs 550€, what yields a total prize of 3300€.

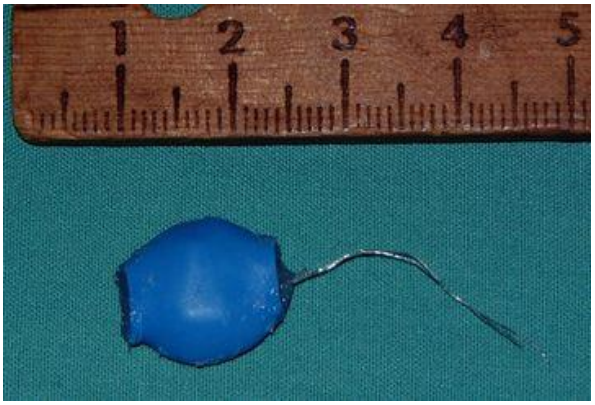

Fig. 1. Harald Stauss implantable nerve stimulator.

Fig. 2. Invilog Ltd. implantable wireless electrical stimulator.

1.8 This BT proposal

In contrast with some of the features of these two already available stimulators, the vagus nerve stimulator that is proposed in this BT (and for the whole series of BTs that is about to start) works in current-control mode and it is designed to deliver passive biphasic pulses with fast reversal. It is switched ON/OFF magnetically and the parameters of the stimulation are aimed to be controlled through IR light. Hence, during its whole process of development it has to be beared in mind that it must keep being wireless and tiny enough to be implantable, what makes it suitable for chronic VNS. Despite there are other alternatives such as inductive coupling, this stimulator is battery powered. Inductive coupling requires more complex and bulkier electronics, so it was rejected. Another alternative would be recharging the stimulator through a wire so that a smaller battery could be utilized, but this would entail subjecting mice to recurrent surgeries. Plus, the final product should be open-source, so that any scientist can modify its performance depending on the needs (e.g. controlling the stimulation parameters magnetically instead of using the IR sensor or changing the circumstances under which its LED has to blink). In addition to the stimulator, it is planned to fabricate cuff electrodes so that both devices constitute a complete pack for vagus nerve stimulation. Therefore, the complete final system will be composed by its implantable building blocks which are the generator, the electrodes and the encapsulation and by an external infrared control system. A sketch of this is showed in *Fig. 3*.

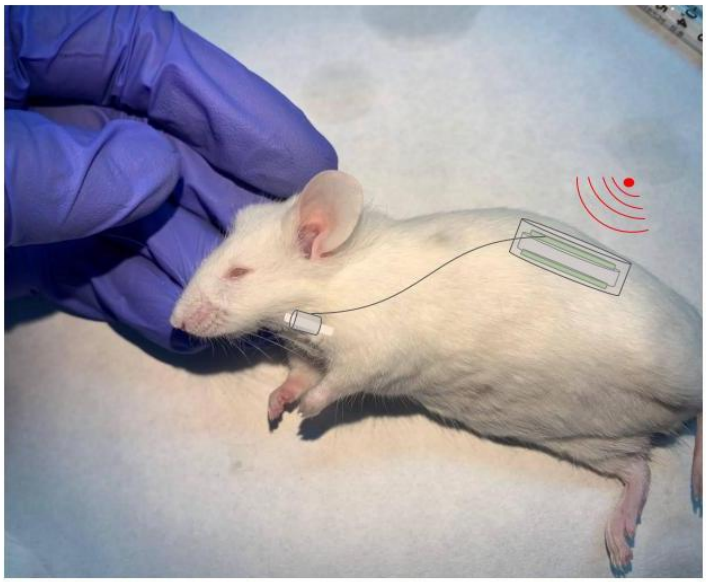

Fig. 3. Global sketch of the vagus nerve stimulation system whose development starts in this BT. Cuff electrodes are planned to deliver stimulation in the cervical region of the nerve, while the generator is expected to be placed in the back. Stimulation will be controlled with an external IR system.

2. MATERIALS AND METHODS

2.1 Stimulator electronics

Several blocks can be distinguished in the whole circuit. In general, the process of selection of the components that make part of these blocks was made in attendance to two requisites, miniaturization and battery consumption. The sketch of *Fig. 4* shows all the building blocks of the implantable stimulator. These blocks are going to be described in depth in the following subsections.

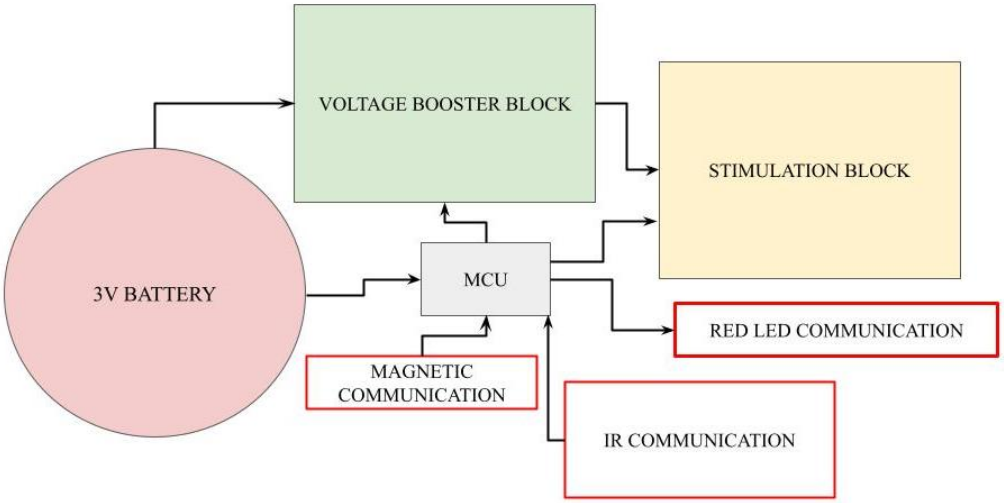

Fig. 4. Sketch of the building blocks of the implantable vagus nerve stimulator that has been designed.

a) Microcontroller

The *Nexperia MKL03Z32* is the microcontroller that is most commonly used to develop miniature systems in the laboratory where this project is carried out (Biomedical Electronics Research Group, Pompeu Fabra University) and it is also included in the design of this stimulator. Its multiple options of low power modes and its availability in a tiny 20-pin WLCSP package (2 × 1.61 × 0.56mm) make it suitable for the purposes of this work.

b) Power source

Since the vagus nerve stimulator that is developed in this work is implantable, the power system is a critical aspect in the process of designing. As it has been previously introduced, this stimulator is battery powered. Thus, the dimensions of the battery are crucial since it is expected to be the biggest component within the stimulator. Rechargeable coin-like batteries with very low capacity have the smallest dimensions available in the market (smaller than 10mm of diameter). However, in order to avoid the drawbacks of these batteries which were commented in the *Introduction*, a primary battery (i.e. a non-rechargeable) battery was selected as the source of power. Primary batteries have much larger energy density capacity than rechargeable batteries. In particular, it was selected the battery model *Renata CR1025* which is a 3V coin battery of 10mm of diameter and 2.5mm of thickness. It is not rechargeable and it has a capacity of 30mAh.

c) Stimulation circuit

As previously introduced, two main types of biphasic stimulation can be distinguished: passive or active. In spite of the fact that some designs for active stimulation have been studied, for instance building an H-bridge with SPDT switches [39] or implanting a Howland current pump [40], all of them yielded too voluminous solutions due to the amount of components involved. As a consequence of this, it was decided to use a method that allows a poorer control of the anodic wave but a much better miniaturization. Hence, by including an in-line blocking capacitor, biphasic passive stimulation with fast reversal (that is the anodic wave unlike the cathodic one is not rectangular but a peak) is aimed to be generated [41]. To obtain it, a cathodic pulse with the current source is delivered first. This pulse charges the dc-blocking capacitor, whose discharge is activated through the electrodes and the tissues. Then, the blocking capacitor is placed at the output of the current source, which is the component that provides to the circuit a fixed current for the stimulation. To accomplish that, *Nexperia PSSI2021SAY*, a current source available in a tiny SOT353 package (2.1 × 1.25 × 0.95mm), has been included [39]. This source reaches up to 50mA of output current (although this at the end depends on the voltage compliance of the stimulation) and can be regulated with an external potentiometer. Precisely, a digital potentiometer is the last component included in this block. In particular, for the design proposed here an Analog Devices AD5290 of 10kΩ maximum is used (4.9 × 3 × 1.1mm). The resistance of this potentiometer can be regulated through a serial peripheral interface (SPI) from the microcontroller and it allows 256 taps (i.e. jumps of 39Ω in this case). This stimulation circuit is depicted in the following sketch (*Fig. 5*).

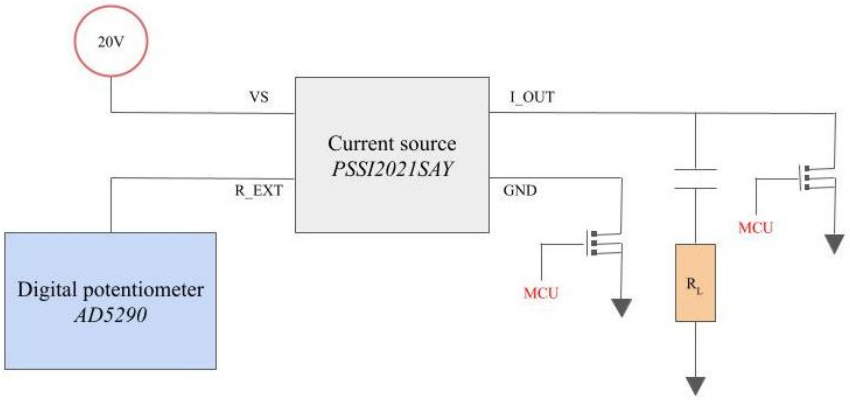

Fig. 5. Sketch of the stimulation circuit.

d) Step-up regulator

As stated in the *Introduction*, in order to ensure eliciting action potentials in the vagus nerve of mice, maximum currents of around 1.5mA are required. As mentioned, with that amplitude depolarization of C-type fibres is not provoked. To guarantee this current amplitude a minimum compliance voltage which depends on the estimated resistance of the electrodes is needed. According to the literature, the calculated impedance of cuff electrodes in cervical vagus nerve stimulation applied to rodents goes from 5kΩ to 15kΩ [42]. Nevertheless, two slight differences can be found between Yaghouby et al. [42] case and this one, namely rats vs. mice and bipolar vs. tripolar cuff. Taking into consideration this impedance by including it in the stimulation simulations performed with LTspice (see *Simulations* subsection) it could be proved that a supply voltage of at least 20V is needed. To achieve that, a step-up regulator must be included in the circuitry of the stimulator. Besides the output voltage, several other conditions have to be accomplished by the step-up converter: availability in a small package, input voltage of maximum 3V (battery supply of the stimulator) and low current consumption. Taking these parameters into account *Maxim Integrated MAX8571* was firstly chosen. Its output can be set from 3V to 28V and it has a shutdown mode (consumption estimated in 0.05µA) and can be purchased in a SOT23 package (3 × 3 × 1.45mm). However, this component does not have a SPICE model and therefore cannot be included in the simulation of the stimulator in order to check its whole behaviour. As a consequence of this, it was decided to look for another converter that allows simulations between the step-up regulator and current source. Finally, *Analog Devices LT3467* was chosen; it reaches up to 40V of output voltage, also includes a low shutdown current (i.e. 0.01µA of typical value) and comes within a DFN package (3 × 2 × 0.75mm). To set its output voltage at the desired 20V, an external feedback circuit must be included.

e) External communication

A way of including bidirectional communication in the device is also taken into consideration so that researchers can check the status of the stimulation. First, a red LED (*Kingbright APG0603SECETT*) is included with the aim of using it to report that status. Therefore, by configuring the number of blinks or the switching frequency it could flash for instance when low battery levels are detected, in order to make the user know the stimulation parameters that are set or when the programmed stimulation session has ended. In combination with this, a way of modifying the stimulation parameters without removing the device from the mouse has to be considered. To do this, an infrared (IR) circuit is proposed. It is composed by an IR photodiode (*Wurth*

Electronik 1540801EEA300), one operational amplifier (*Analog Devices ADA4505-1*) and some of the capabilities of the microcontroller needed to read the input signal. This photodiode comes within a 0805 package (2 × 1.3 × 0.8mm) and has a photo current consumption of 1µA. Finally, so that after implantation the stimulator can be awakened from a default sleep mode, a digital switch Hall Effect sensor (*Texas Instruments DRV5032)* is incorporated [40]. Hence, the output of this device will be connected to a GPIO pin of the MCU set at *input* mode. With that, the microcontroller can be magnetically switched ON/OFF. Plus, the advantage of using this sensor in particular is its low current consumption (1.6µA at 3V of power supply). Another advantage of this sensor over other alternatives which were studied such as a simple magnetic reed switch (which would not consume any current at all) is its tiny packaging: 1.1 × 1.4 × 0.4mm. When compared with the size of the smallest magnetic reed switch found (*Cynergy3 VDA200H*), which is 5.4 × 1.4 × 1.4mm, the volume of the Hall Effect sensor is 17 times smaller.

If some zoom in was applied to the implantable pulse generator of *Fig. 3*, something similar to what can be appreciated in *Fig. 6* would be seen. This sketch takes into consideration the thickness of the most relevant components that have been chosen in the design process detailed above.

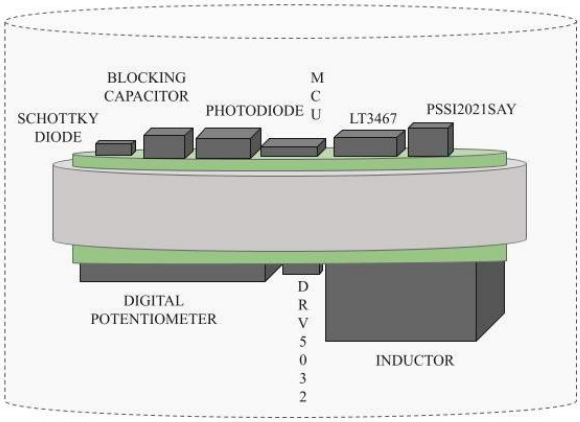

Fig. 6. Appearance of the encapsulated vagus nerve stimulator that would be implanted into the mouse. The battery is coloured in light gray, two PCBs are coloured in green and the biggest components of the device are coloured in dark gray.

2.2 Simulations

SPICE simulations were carried out with Analog Devices LTspice XVII Simulator. Two key components were tested in LTspice, the step-up converter LT3467 and the current source PSSI2021SAY. Their couple performance was also evaluated. As it was mentioned above, the estimated impedance of the electrodes which is needed to perform the simulations was obtained from [42] and was then set at 12kΩ. Obviously, all the values of the external components (capacitors, inductor etc.) used for the simulations match with the values of the components included in the PCB.

2.3 PCB design

Once all the needed electronic components were identified and selected, two printed circuit boards (PCBs) were designed. One for the implantable vagus nerve stimulator and another one for its evaluation board (i.e. “big vagus nerve stimulator”). To do so the

software EAGLE 6.5.0 (*Cadsoft Computer GmbH*, currently part of *Autodesk Inc.*) was used.

2.4 Physical implementation of the stimulator circuit

Due to time constraints only one of the two designed boards was ordered, the evaluation board, which is required first in order to study the behaviour of the components. The evaluation board was manufactured by Eurocircuits and consisted in a 2-layer class 6 base copper board. All the components were manually welded onto the board, either by using soldering flux tack (*Chipquick, SMD291*) and an IR reflow oven for the smallest ones (e.g. the Schottky diode or the MOSFET transistors) or simply using a soldering iron (*Weller*) and tin roller (*Loctite 309, 0.5mm*).

2.5 Electrodes design and manufacture

For the fabrication of the cuff electrodes two methods have been studied; one based on the process proposed by Emily L. Foldes et al. [43] to manufacture cuff electrodes with suture, and the other one based on the proposal of Gregory G. Naples et al. [44], where how to build a spiral cuff is detailed. Finally, the first one of these two methods was chosen, the reasons were: a lower complexity in the process of manufacture, the steps to follow are better detailed and time constraints This process was slightly modified in order to fit the available resources and to try different approaches, hence leading to a simplification.

a) Preparation of the metal contacts

Design

The design of the manufactured electrodes is based in a tripolar configuration, which consists in a central cathode and two flanking anodes. The aim of this distribution is to avoid the formation of virtual cathodes outside of the cuff, which is more bound to happen if a bipolar configuration is adopted instead [45]. The conflict generated by virtual cathodes is that depending on the magnitude of the stimulation they can also generate undesired action potentials that are not under the control of the stimulator. Even so, it has to be taken into account that, as it is going to be shown in the following steps, the anodes of the electrodes that are fabricated for this work behave the same way. This is remarkable since another approach is isolating the anodes in order to apply different currents on them. Therefore, the direction of the generated action potential aims to be better controlled. For instance, if action potentials are desired to travel in the orthodromic direction (towards the terminal of the axon) the anodic current applied in the anode that is in the antidromic direction (closer to the soma) is set at higher amplitude than in the other anode. As a consequence of this, it is intended that the first anode produces an arresting current so that it blocks antidromic stimulation [45]. This cannot happen with these electrodes.

Fabrication

Platinum foil (*Goodfellow, PT000235*) was acquired. The dimensions of the foil are 50 × 1.2 × 0.0025mm and it has a purity of 99.95%. From this rectangular foil, tripolar electrodes are trimmed. Regarding the dimensions of the electrodes they have a surface of approximately $1mm^2$, with 1.2mm of width (that is the full width of the foil) and around 0.8mm of length per pad. This width allows the electrodes to accomplish with the criteria indicated by L. Foldes et al. [43], according to which it should be between π and 2π times the diameter of the target nerve. Since cervical vagus nerve in mice has a

diameter of around 0.3mm [21], 1.2mm fits in the range 0.942mm – 1.884mm. Moreover, the interpolar distance used for the manufacture of the electrodes is 2mm [36]. In order to cut the platinum so that the desired shape can be obtained, a blade is used (*Feather P-745*). However, due to the hardness of the metal, it is recommended to start by using the blade rather like a punch, using its tip to drill the platinum to mark a bit the cut lines. Just sliding the blade over the platinum may not be enough to cut it properly. Once the cut lines are better marked thanks to the drilling, it is easier to trim the metal and to bend it by the lines so that the objective can be accomplished.

b) Soldering

Once the platinum electrodes have been cut, they can be soldered to the wires that will connect the stimulator and the electrodes. As it has been introduced previously, this electrodes use two wires, one for the cathode and another one for the two anodes, which should behave identically. To do so, multi-stranded stainless-steel type 316 wires (*A-M Systems, 793400*) are used. These wires are coated with *Perfluoroalkoxy alkanes* (PFA), so they are already insulated. Additionally, it is crucial that they are flexible enough so that they can travel from the cervical region of the mouse, where the cuff electrodes are expected to be placed, to its back, where the stimulator is expected to be implanted. Before starting to solder the wires to the platinum, their tip is stripped removing the coating. Despite in the original paper [43] a spot welder is utilized for this operation, in this case a laser-welding machine (*Sisma LM-D180*) is used instead. The wires can be soldered in two ways, either radially with respect to the electrodes or axially. In this work they have been soldered axially, which is hypothesized facilitates the later process of silicone curing when preparing the cuff, making more difficult for the sheets to unglue.

c) Sandwiching

Finally, the platinum electrodes must be covered by the cuff. With that purpose, two sheets of silicone MED82-5010-10 (*NuSil, Avantor*) with 25µm of thickness are used. Due to issues with the distributor of the sheets and delivery dates, MED82-5010-10 sheets have been used instead of MED92-5010-10, which are not restricted to 30-days implanted and therefore should be the ones used in this case since they allow chronic stimulation. Plus, to glue the two sheets (upper and bottom) to the electrodes, MED-1137 (*NuSil, Avantor*), a one part, low slump, solvent free translucent silicone, is utilized. This silicone cures at room temperature and needs at least 72 h. Also on the contrary with respect to what is indicated in the paper, this silicone is used to stick both the platinum to the silicone sheets and the silicone sheets between themselves. Originally, MED-1137 is used for the interface platinum-silicone sheets and a silicone elastomer (MED-4211, *NuSil, Avantor*) for the interface silicone sheet-silicone sheet. As well in this case, issues with the distributor conditioned this decision. Regarding the dimensions of the cuff, as pointed out in M. Noller [21] work, in a pseudo-tripolar configuration such as the one designed here, the distance between the last electrode and the end of the cuff is not a great concern. Here, 2 mm of gap are given at each side between the platinum array and the cuff, yielding a total size for the cuff of approximately 10 × 5.2mm.

To prepare the sandwich that will compose the cuff, three different methods have been tested. In a first trial, two sheets of the previously mentioned dimensions are first trimmed. Then, MED-1137 is spread over the bottom sheet and the already-welded-to-the-wires platinum electrodes and the upper sheet are placed onto it. After three days curing the cathode is isolated from the anodes by physically cutting it with a blade and

windows are opened in the sheet contrary to the wires so that the electrodes can deliver current to the nerve. This approach showed several disadvantages. First of all, to start working with the sheets already with their final dimensions proved to be a trouble when trying to glue the upper one to the bottom one, since due to their small size it is difficult to exactly align them. Moreover, once the electrodes are properly sandwiched and the silicone has cured, two more problems show up. On the one hand, opening the windows only by removing silicone from the upper sheet without damaging the electrodes below is pretty hard. On the other hand, when isolating the cathode in the middle of the electrodes, the exerted force used to cut the platinum below the silicone can move the sheets and misalign the two layers of the sandwich.

To deal with these problems a second approach has been tried. This alternative simply consists in using a bigger size for the sandwich (e.g. three times bigger yielding a first cuff of around 30 × 14mm). Although this is really helpful when aligning the sheets in the gluing phase and when isolating the cathode since the movements produced can be later corrected by trimming the cuff to its real dimensions, opening the windows for the electrodes leads to the same trouble, the platinum below gets damaged by the blade.

As a consequence of this, a third methodology is thought up. A sketch of the final process, which is going to be described in the following lines, is depicted in *Fig. 7*. In this case the idea of the second approach is still conserved but additionally the windows are opened before fabricating the cuff. Thus, in the sheet that is going to be used as the upper one, three windows are opened at the same distance that the three electrodes have in the platinum that is going to be sandwiched. In order to reduce the difficulty of cutting the windows at their exact points without having the reference of the electrodes below, the opened windows are a bit bigger than the ones actually needed by the electrodes. In this way, even if little misalignments are produced when placing the upper sheet onto the platinum and the bottom sheet, the windows still match the electrodes. The empty spaces produced by this technique are later corrected by filling them with silicone. Therefore, in this case the only thing that has to be done once the silicone has cured into the sandwich is isolating the cathode. The gap produced by the blade when cutting it is also refilled with silicone. As in the second approach, once this has been done the cuff is trimmed to its real dimensions.

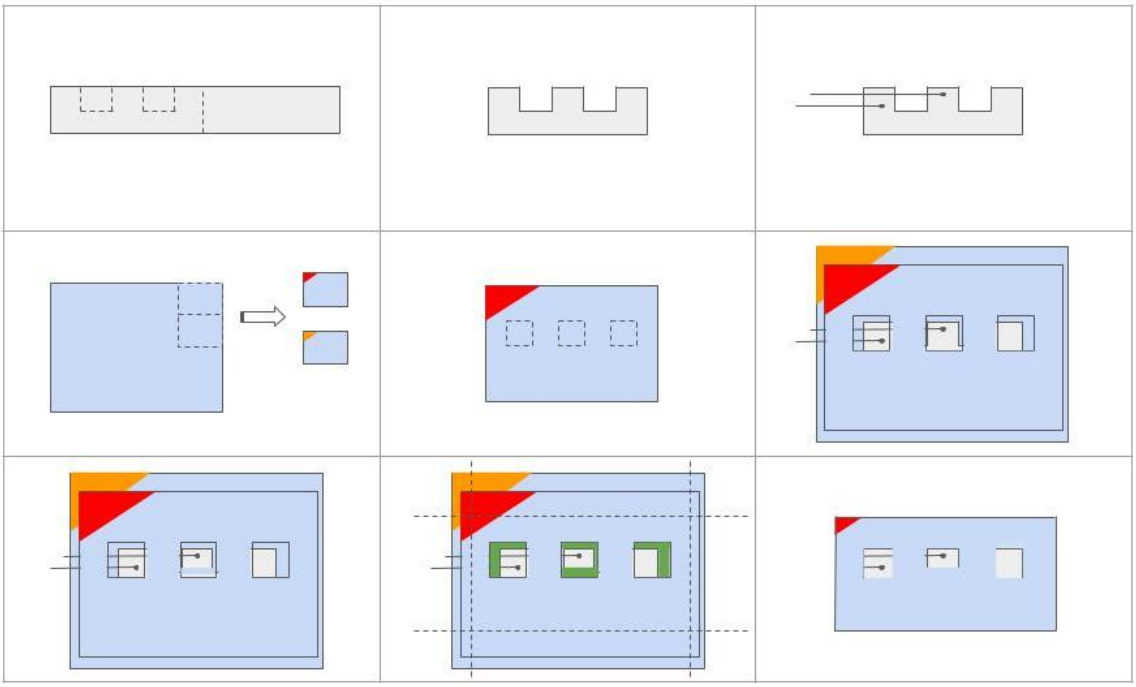

Fig. 7. Sketch of the final process of manufacture of the cuff electrodes.
Steps are ordered from top to bottom and left to right. 1 & 2: electrodes are trimmed from the platinum. 3: the wires are soldered to the electrodes. 4: Two silicone sheets are trimmed for the cuff (bottom-orange, upper-red). 5: Windows for the electrodes are opened in the upper sheet. 6: Electrodes are sandwiched. 7: The cathode is isolated from the anode. 8: Gaps are filled with silicone (green) and the cuff is trimmed to the desired dimensions. 9: Final aspect of the cuff.

2.6 Circuit design

The schematic of the designed stimulator circuit (evaluation board version) is represented in four different sketches compose the design of the evaluation board. The first one of them, which is attached in *Fig. 1* of the *Supporting Information* section, contains five blocks which, from left to right and top to bottom, are: the battery holder, the DRV5032, the Serial Wire Debug (SWD), the MCU input capacitances and the MCU itself. As it can be noticed, a jumper is placed at the output of the battery holder so that current consumption of the whole device can be monitored along time. This is going to be something really common in the evaluation board of this vagus nerve stimulator where, as it is going to be showed from now on, all the components have at least one jumper at their input pin in order to monitor their current consumption. The aim of this is establishing a classification which ranks all the components from more to less power-hungry so that those ones which require more power can be kept switched off as much time as possible.

The sketch of *Fig. 2* in the *Supporting Information* section shows the step-up converter and its external components. Its output voltage is fixed at 20V thanks to the value of the feedback resistors, which are chosen according to this objective. In addition to that, the values of the capacitors, the Schottky diode (*ON Semiconductor NSR10F40NXT5G*) and the inductor (*Abracon ASPI-4030S-100M-T*) are chosen following the advice given in the data sheet of the device. As it can be appreciated, in this case not only a jumper devoted to measure the current consumption of the component is included, but also another one with three pins which allows the user to

control the step-up through its SHDN pin without having to program the microcontroller.

In *Fig. 3* of the *Supporting Information* section, the sketch of all the components that directly provide stimulation (namely the potentiometer and the current source) is showed. At the left, the potentiometer is configured in rheostat operation, that is the wiper and its A pin are connected together to 20V, and its B pin is connected to the REXT pin of the current source. The four pins of the potentiometer devoted to its configuration through SPI are also connected to jumpers so that the device can be configured externally (e.g. with an Arduino). This can help to test the device without programming the MCU previously. Another important role is carried out by the jumper connected to A/wiper and B terminals, which allows using an interchangeable external resistor to set the stimulation current managing without the potentiometer. Finally, note that, also according to layout recommendations, four bypass capacitors are added between VDD and VSS. In fact, it is advised that two of these capacitors are made of tantalum instead of ceramic. However, tantalum capacitors entail the disadvantage of having a bigger size than ceramic capacitors, which is something quite undesired for the purpose of this stimulator. Therefore, two jumpers have been placed besides the tantalum capacitors, so that they can be disconnected from the circuit and the behaviour of the potentiometer can be tested without them. Due to their size, managing without them would be an interesting alternative. Moving on to the right part of the sketch, the PSSI2021SAY is supplied with 20V and it is connected to the potentiometer, which determines its output current. In order to control the switching of the source so that it can only be activated when it is desired to deliver pulses, a MOSFET and a BJT connect the device to ground. Both transistors have been added to establish a comparison between the behaviour and the current consumption of each one of them. Since the current source does not have a pin to set it in a shut-down/sleep mode, the role of this transistor is essential to control the cathodic pulse of the stimulation. The output anodic pulse works thanks to the previously mentioned blocking capacitor and to another MOSFET, plus this can be measured with another jumper. Also, all the gates of the transistors are connected to a jumper with the aim of being able to switch them on externally without having to program the stimulator first.

The fourth block, which is displayed in *Fig. 4* of the *Supporting Information* section, simply contains the circuit of the LED and the one of the photodiode. The output of the IR photodiode is connected to a pin of the MCU with comparator (CMP) capability. Hence, the value measured at this pin is compared with the one measured at another CMP pin, which obtains its input from the output of another MCU pin with V_REF functionality. It also has to be mentioned that the photodiode is powered from a GPIO pin of the MCU, since connecting it directly to the battery would not be efficient at all from a current consumption perspective.

Finally, *Fig. 8* and *Fig. 9* respectively show the aspect in EAGLE of the PCBs of the evaluation board of the stimulator and its implantable version. While the board of the bigger version (80 × 60mm) only needs two independent copper layers (i.e. top and bottom), for the implantable version (10mm of diameter) 5 layers are required (top, bottom, 3V, 20V and GND) to fit all the components in a PCB that matches the diameter of the coin battery. To achieve that degree of miniaturization, the components of the implantable vagus nerve stimulator are distributed on the top and bottom layers of the PCB, which is stacked to the battery. Apart from that, the dimensions of the packages are the only difference between both boards. For instance while 0805 package was chosen for resistors or capacitors of the evaluation board, for its implantable version 0201 packages are proposed (as long as they fit other requirements, e.g. forward

voltage). This miniaturization challenge is represented in *Table 1*, which ranks the dimensions of all the components used for the implantable vagus nerve stimulator. In fact, the tantalum capacitors are not included in the design of *Fig. 9* because their size is unacceptable for the constraints of the implantable version of the stimulator. Therefore, determining with the evaluation board if these capacitors are completely essential or not, is one of the different possibilities that that board offers. Emphasise was also made in distributing the external components of the step-up converter according to the recommended layout specifications, since ensuring a stable 20V output is crucial for the stimulator. Finally, avoiding laser drilling microvias in the fabrication process is an important point to take into consideration when designing a PCB with components with interior pins such as current MCU. Otherwise, the cost of fabrication of the device gets more expensive, limiting its future use as an open-source stimulator. Following this premise, the sketch of *Fig. 10* shows how the different pins of the MCU in the implantable version are configured according to their possible functionalities and stimulator needs. As it can be appreciated there, it is unavoidable to use at least one of the central pins so that all the capabilities of the stimulator can be implemented.

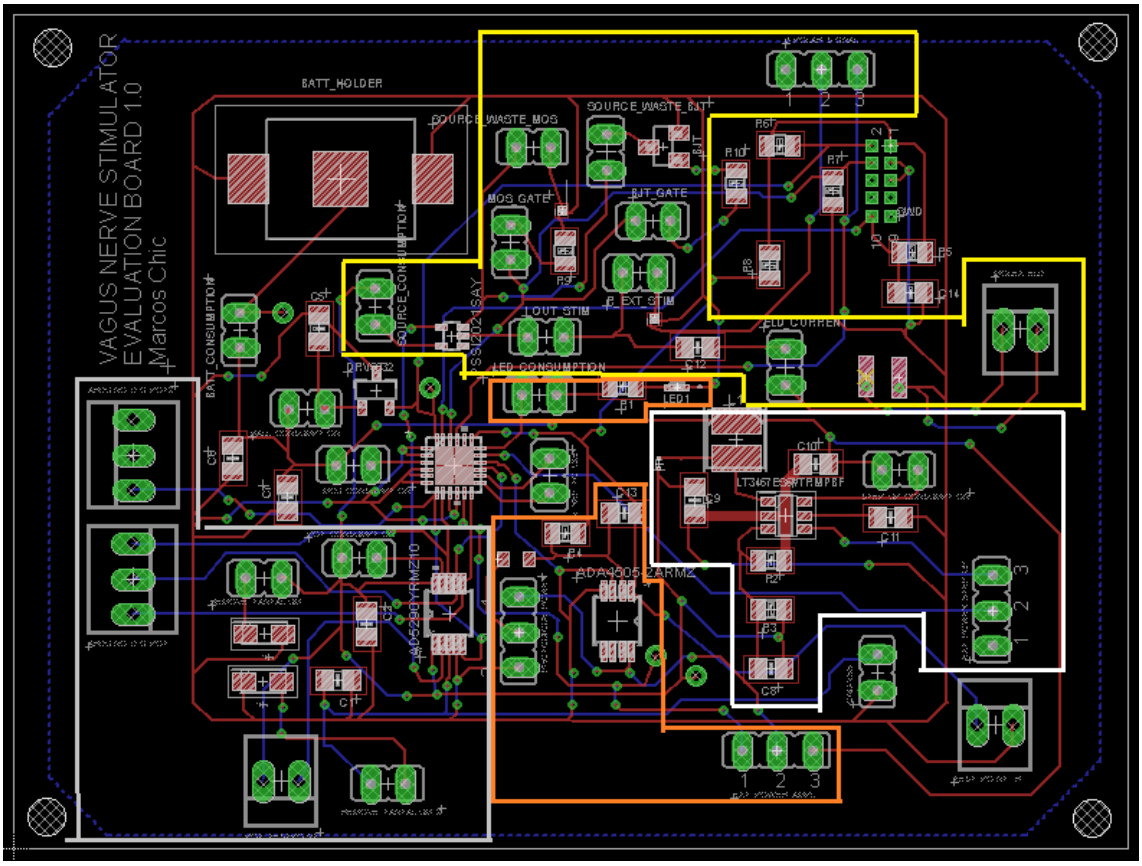

Fig. 8. Final design of the evaluation board of the vagus nerve stimulator. In the yellow area the PSSI2021SAY circuit, in the white area the LT3467 circuit, in the orange area the LED (upper) and the photodiode (bottom) circuits, in the gray area the potentiometer circuit, in the middle of the board the KL03 and besides it the DRV5032. At the top left corner a battery holder can be found.

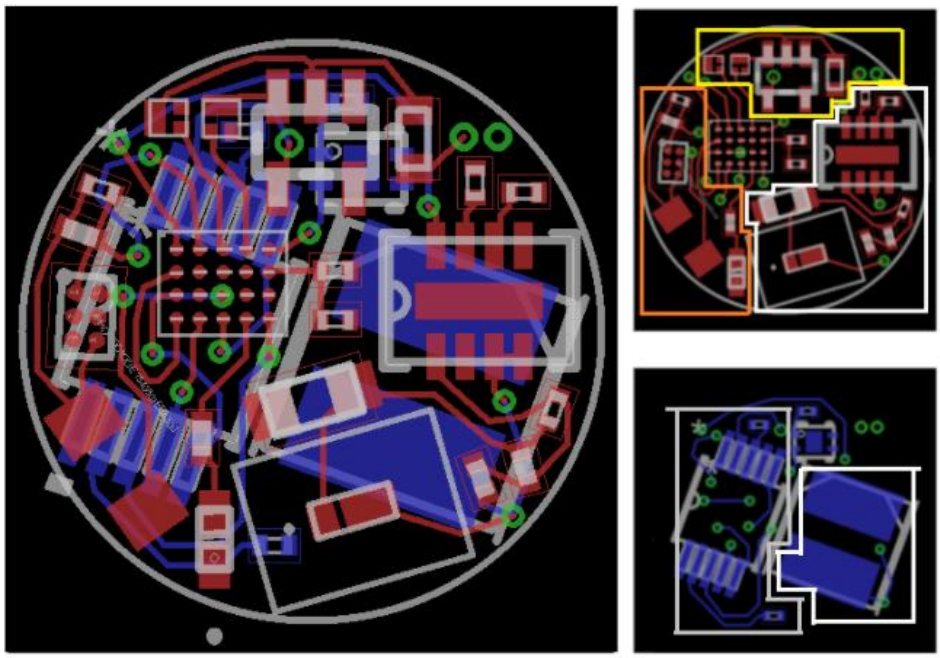

Fig. 9. Beta design of the implantable vagus nerve stimulator. Right top image only shows components at top layer, right bottom image only shows bottom layer. The colour code used to mark the different blocks is the same as in Fig. 1. The big component at top which is not marked is the KL03, while the one not marked at bottom is the DRV5032. Note that since this version was not fabricated and it may be still open to changes, layers are not placed.

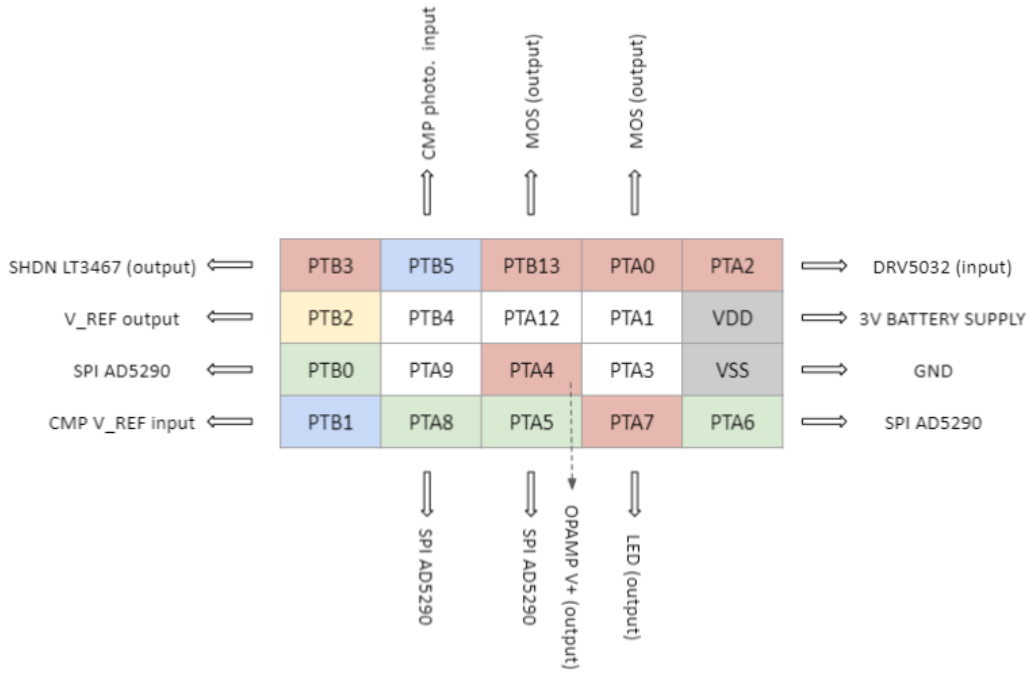

Fig. 10. Sketch of the design of the MCU pins for the WLCSP package of the implantable version. Legend: RED – GPIO functionality, BLUE – CMP0_IN functionality, GREEN – SPI0 functionality, YELLOW – V_REF_OUT functionality.

Component	Description	Dimensions (mm)
Renata CR1025	Battery	10 (d) × 2.5
Abracon ASPI-4030S-100M-T	Inductor	4 × 4 × 3
Analog Devices AD5290	Digital Potentiometer	3 × 4.90 × 0.85
Analog Devices LT3467	Boost converter	3 × 2 × 0.75

Nexperia PSSI2021SAY	Current source	2.1 × 1.25 × 0.95
Kinetis KL03	Microcontroller	2 × 1.6 × 0.56
Würth Elektronik	Photodiode	2 × 1.3 × 0.8
Capacitors	0603 package	1.6 × 0.8 × 0.8
Analog Devices ADA4505-1	Operational Amplifier	0.9 × 1.38 × 0.6
Texas Instruments DRV5032	Hall Effect sensor	1.4 × 1 × 0.4
ON Semiconductors NSR10F40NXT5G	Schottky diode	1.4 × 0.6 × 0.3
Vishay 298D106X0025A2T	Tantalum capacitors (if needed)	1 × 0.6 × 0.5
Capacitors	0402 package	1 × 0.6 × 0.2
Diodes Incorporated DMN2990UFZ	MOSFET transistors	0.62 × 0.62 × 0.39
Kingbright APG0603SECETT	LED	0.65 × 0.35 × 0.2
Capacitors/resistances	0201 package	0.6 × 0.3 × 0.24

Table 1. Classification of the components of the implantable vagus nerve stimulator by their size.

3. RESULTS

3.1 Simulations

The performance of two key components of the stimulator has been simulated both independently and jointly. Simulations with the LT3467 can be appreciated in *Fig. 11*, where the step-up converter turns a 3V input into a 20V output. 20V are reached in less than one millisecond and the step-up converter is switched on/off through its SHDN pin with a period of 20 milliseconds (see *Discussion* for an explanation).

Fig. 11. Simulation of the behaviour of the LT3467 when being configured to output 20 V.

Plus, *Fig. 12* shows the current travelling through the electrodes in the PSSI2021SAY simulation. In this case, since the digital potentiometer does not have an LTspice model, the *Rext* pin of the current source is simply connected to a resistance. In this simulation real conditions for vagus nerve stimulation are implemented, which means a 20Hz frequency and a pulse width of 500µs (check *Introduction* section).

These parameters are controlled through the type of pulses applied at the gate of the MOSFET transistor which connects the source to ground and therefore switches it on/off. The other MOSFET allows the 1µF blocking capacitor to discharge and therefore generates the anodic phase of the pulse. Thus, with the value of the external resistance set at 200Ω and a supply voltage of 20V, stimulation pulses of around 1.6mA are obtained.

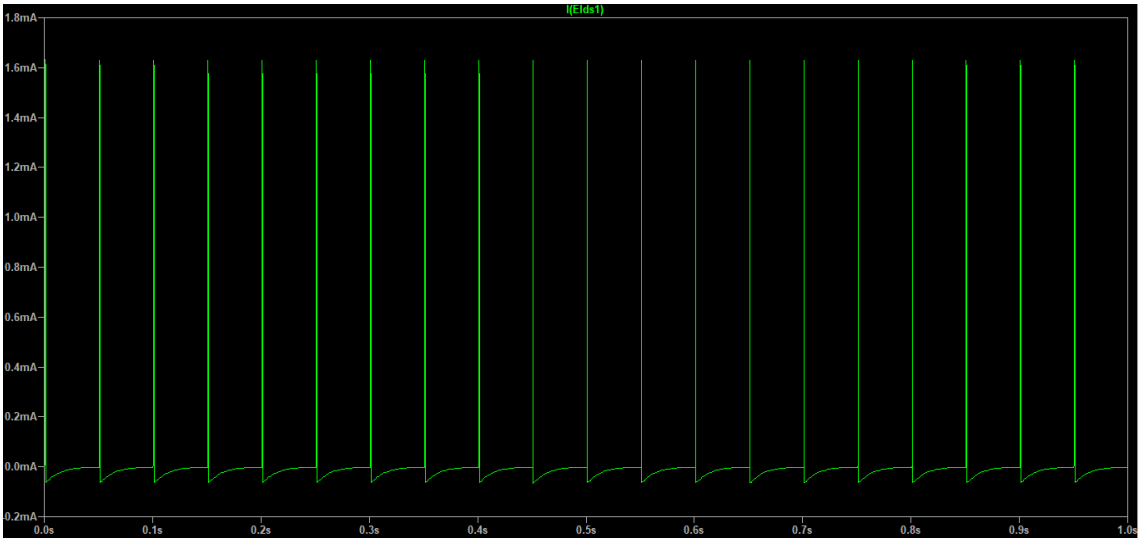

Fig. 12. Simulation of the output current of PSSI2021SAY when it is supplied by an independent voltage source.

Finally, in the simulation of *Fig. 13*, the performance of the two previously mentioned components is evaluated together. Due to computational limitations the image shows a 1 second cycle of stimulation. Nevertheless, as mentioned in the *Introduction*, current standard duty cycle for instance for epilepsy consists in 30 seconds of stimulation and 5 minutes of rest.

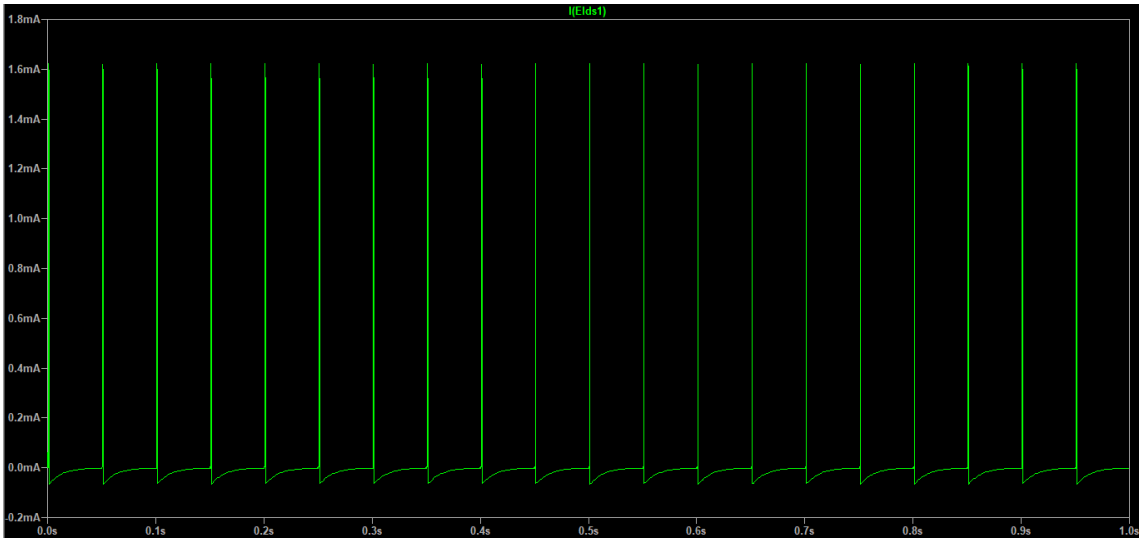

Fig. 13. Simulation of the current delivered by the stimulator to the electrodes. Here the PSSI2021SAY is supplied by the LT3467.

To better understand the timings of the stimulation circuit that has just been referred, *Fig. 14* shows the timeline of the configured stimulation with the switching times of its components.

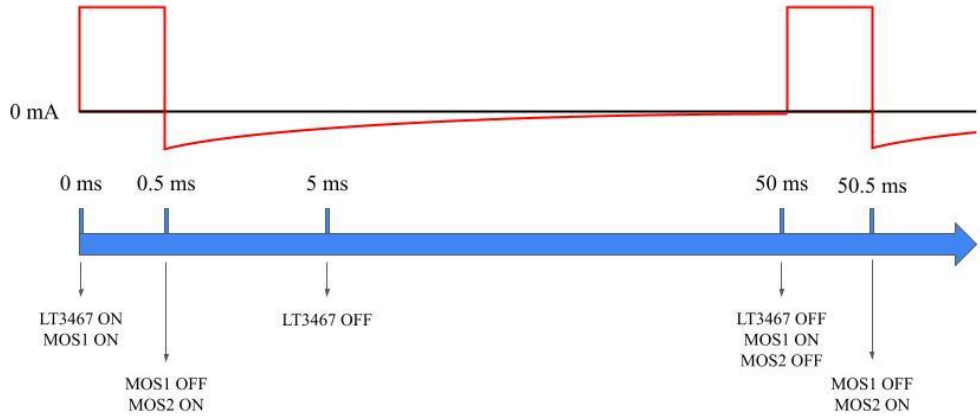

Fig. 14. Stimulation timeline. Note that time and current are not to scale. Also, an explanation to the switching time of the LT3467 is provided in the Discussion.

3.2 Stimulator fabrication & performance

Fig. 15 shows the already-fabricated evaluation board of the vagus nerve stimulator and *Fig. 16* shows the assembled board. As it can be noticed in that last image, there are a few components of the evaluation board that are not mounted; the AD5290 and part of the external circuitry of the photodiode (i.e. feedback resistor and capacitor and configuration jumper). The digital potentiometer has not been mounted since it is not essential to make the current source work (an external resistor can be used instead) and programming it would have required some time. On the other hand, since in present work the programming of the stimulator is not reached, welding the photodiode and its external components taking into account their role in the stimulator was not considered a priority.

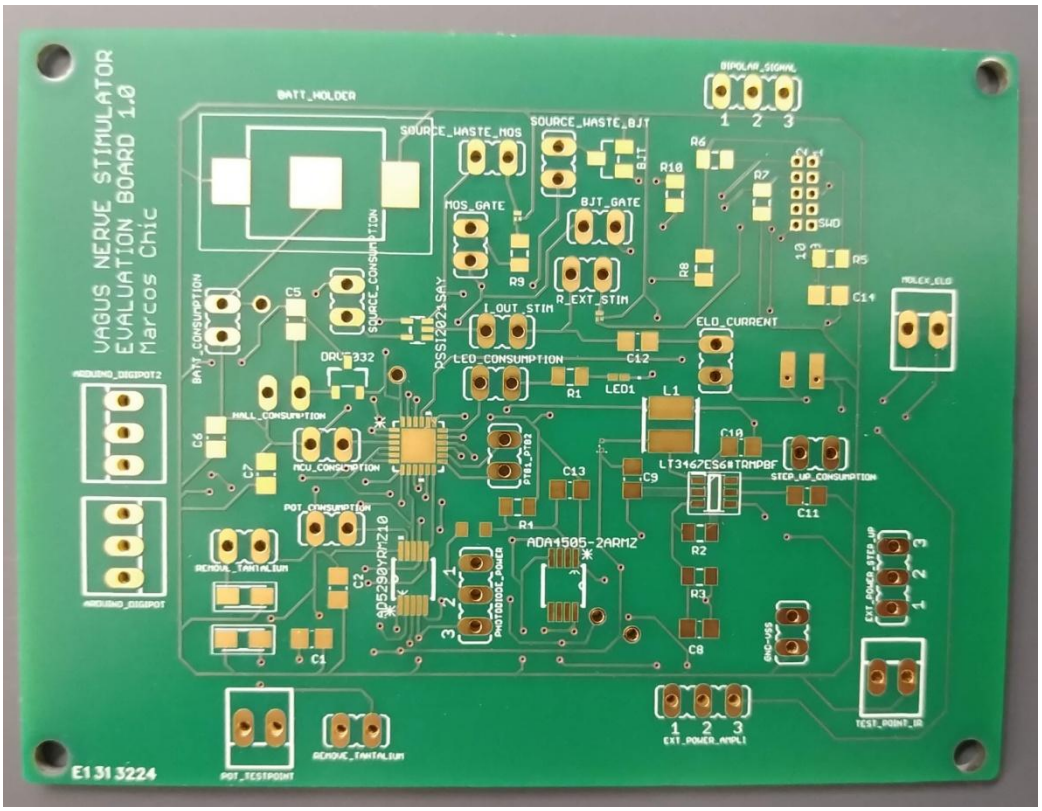

Fig. 15. Fabricated evaluation board of the vagus nerve stimulator.

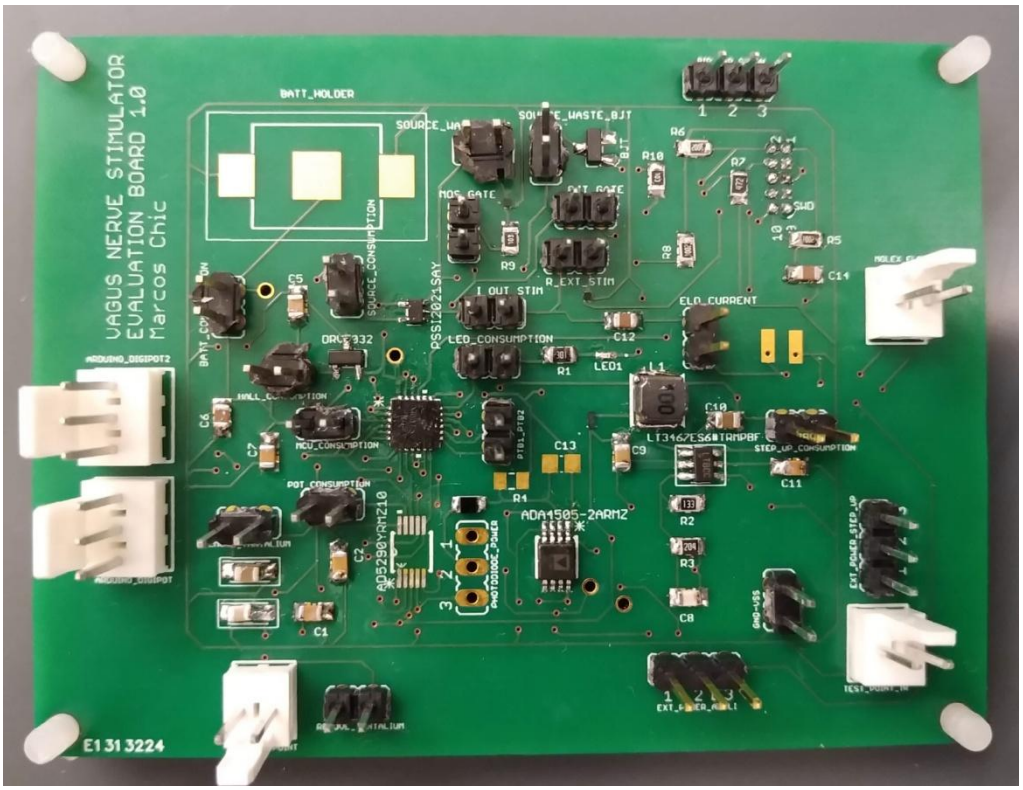

Fig. 16. Fabricated evaluation board of the vagus nerve stimulator with its components assembled.

Furthermore, the performance of some blocks of the stimulator has been tested. The step-up converter was proved to successfully output 20V when having an input of

3V, which validates its chosen external components. In addition to that, the LED also proved to work properly. Finally, since the current source performance was also tested successfully, it has been tried to create a real stimulation shape wave by controlling the MOSFET transistors with an Arduino Uno and supplying the current source with an external voltage source set at 20V. This led to the results of *Fig. 17*, where an oscilloscope (*Hantek DSO1202S*) measures the voltage at the 12kΩ output resistance that simulates the impedance of the electrodes. As it can be appreciated there, 20Hz pulses with an amplitude in the cathodic phase of 1.56mA (18.8V / 12kΩ) are generated. An external 200Ω resistance has been used to configure the source (i.e. this is the resistance that would be set at the potentiometer), hence these results correlate quite well with the performed simulations of *Fig. 12* where a 200Ω external resistance was also used and a similar output is obtained. *Fig. 17* also shows the discharge of the capacitor which provokes the anodic phase. Moreover, as it can be noticed in *Fig. 18*, the pulse width is the desired, 500µs.

These experiments also yielded to the results showed in *Table 2*, where the independent current consumption in permanent regime of some components is ranked. Moreover, the response of the output current of the PSSI2021SAY to different external resistors was also measured and it is described in *Table 3*.

Component	Description	Consumption (mA)
Analog Devices LT3467	Boost converter (ON state)	17.99
Kingbright APG0603SECETT	LED	3.92
Nexperia PSSI2021SAY	Current source (ON state)	0.454
Diodes Incorporated DMN2990UFZ	MOS of current source GND	0.376
	BJT of current source GND	0.374
Nexperia PSSI2021SAY	Current source (OFF state)	0.079
Analog Devices LT3467	Boost converter (SHDN state)	0.012
-	Basal consumption 3V capacitors	0.013
Texas Instruments DRV5032	Hall Effect sensor (OFF state)	0.001

Table 2. Current consumption in permanent regime of some components of the vagus nerve stimulator.

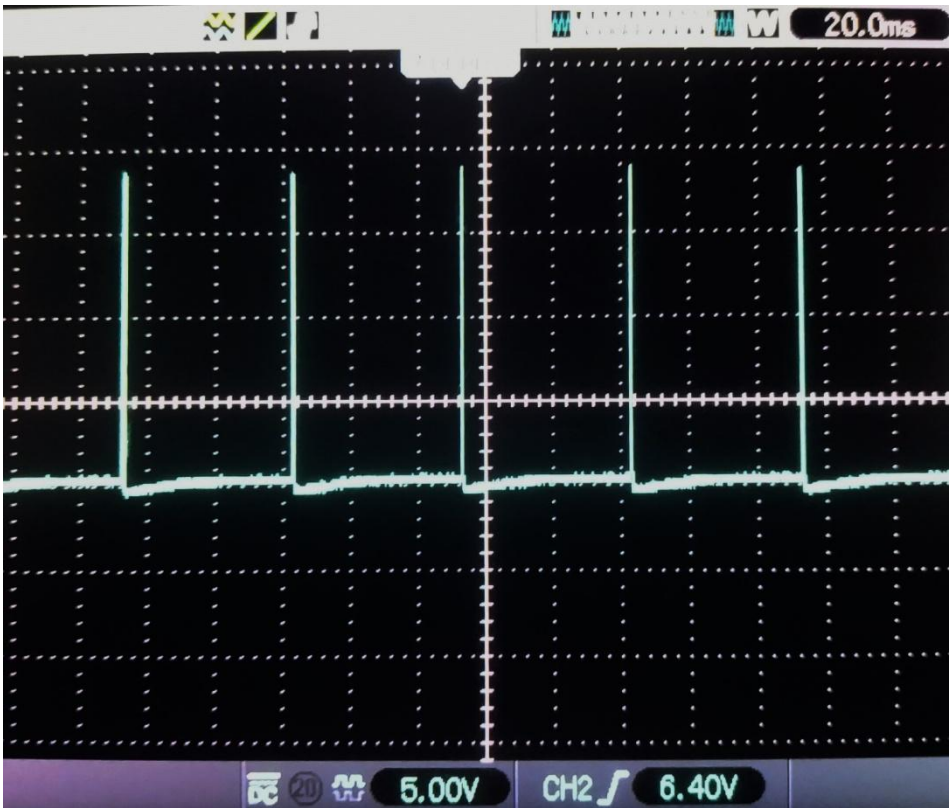

Fig. 17. Voltage at the output 12kΩ resistance when the source is programmed to deliver 500 μs pulses at a 20Hz frequency.

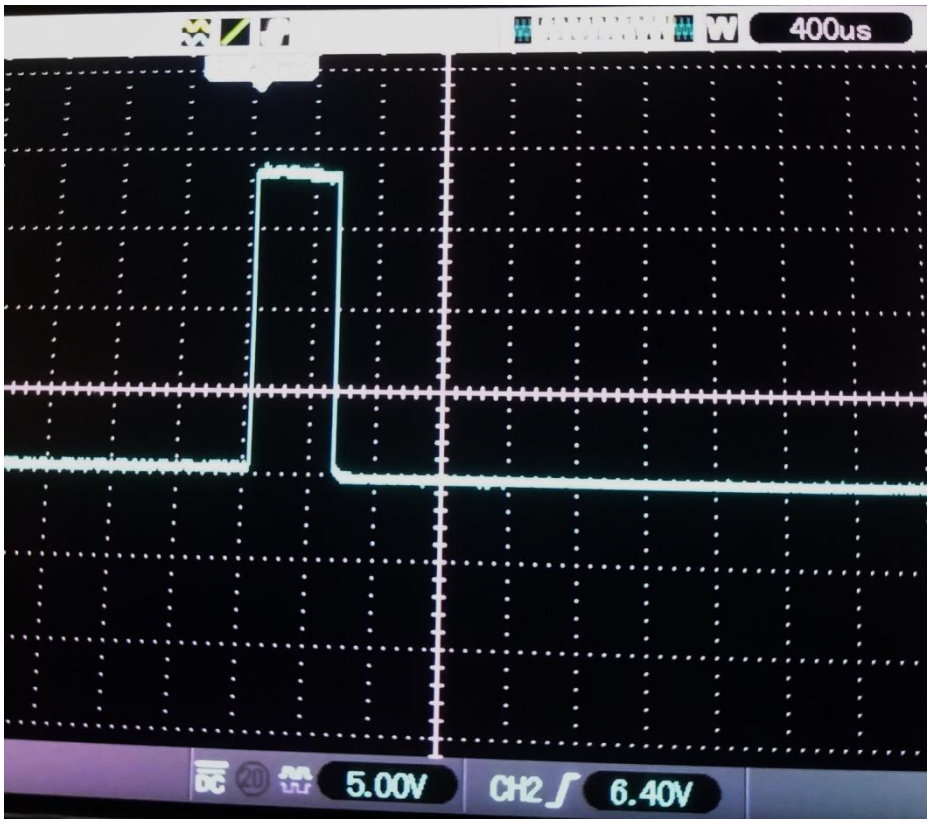

Fig. 18. Zoom applied to one of the pulses of Fig. 9.

External resistance (Ω)	Output current (mA)
6800	0.133
2200	0.370
1300	0.606
620	1.226
200	1.649
100	1.665

Table 3. Response of the output current controlled by the PSSI2021SAY to different external resistances Conditions: 20V of supply and output resistance of 12kΩ.

Finally, it has also been evaluated how changes in the impedance of the electrodes (i.e. changes in the value of the output resistance that simulates them) affect the output current. The conditions for this experiment were also a 20V external voltage supply and a 200Ω external resistance to configure the current source. The obtained results are showed in *Table 4*, were the real value of the used load resistances is also included. This value was measured with a LCR meter (*RS Pro LCR-1703*). Moreover, since the output current was actually obtained from the voltage at the load resistance measured with the oscilloscope, this value is also included. The values of the column referring to the expected output current were obtained from the LTspice model of the circuit. In addition to this, *Fig. 19* graphs how the measured output current decreases as the load increases and how the measured values correlate with the expected ones.

R_L (kΩ)	Measured true R_L (kΩ)	V_R (V)	Measured I_{out} (mA)	Expected I_{out} (mA)
1	1.00 (48%)	3.6	3.6	3.56
2	1.99 (8%)	6.96	3.48	3.56
5.1	5.08 (24%)	17.8	3.49	3.54
7.5	7.5 (36%)	18.6	2.48	2.58
10	9.96 (48%)	18.8	1.88	1.94
12	11.93 (56%)	18.8	1.56	1.62
15	14.9 (72%)	18.8	1.25	1.29
20	19.86 (8%)	18.8	0.94	0.97
30	29.8 (12%)	19	0.63	0.65
39	38.89 (16%)	19	0.48	0.5
51	50.82 (24%)	19.2	0.37	0.38
62	61.99 (28%)	19.2	0.3	0.31
75	74.95 (36%)	19.2	0.25	0.26
100	99.72 (48%)	19.2	0.19	0.19

Table 4. Changes in the output current as the load resistance increases.

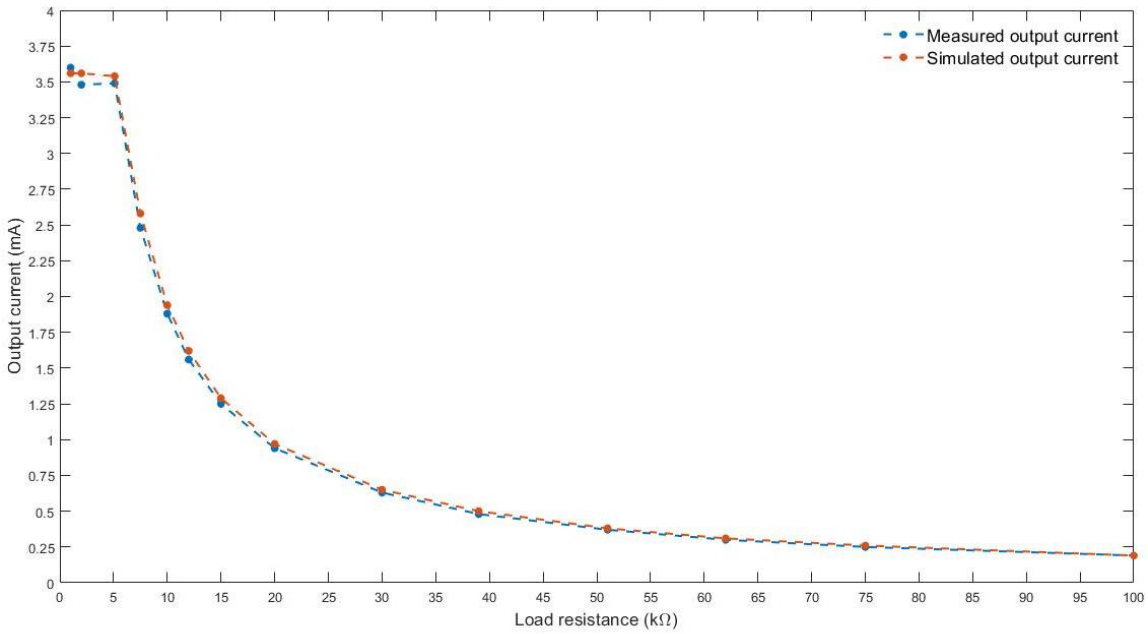

Fig. 19. Measured and simulated output currents vs. load resistance.

3.3 Electrodes fabrication

The results of the first step of the process can be appreciated in *Fig. 20*, where the already trimmed platinum tripolar electrodes are showed. Despite at this point all of them are still connected, as it has been introduced before the central pad will act as cathode and the two flanking ones as anodes. Note the irregular edges in the electrodes, which prove the hardness of the platinum even having been cut with a new blade.

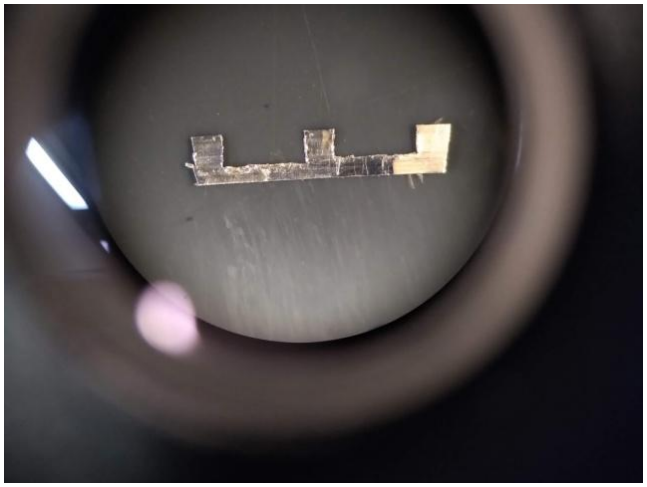

Fig. 20. Platinum electrodes trimmed from the original foil.

In *Fig. 21* the stainless steel wires have already been soldered to the electrodes. Since the two anodes will remain connected, there is no need of soldering a different wire to each one of them. This step is performed utilizing the laser welding machine and means a really delicate phase, since this machine can produce holes in the platinum when soldering the wires to it and can therefore reduce the contact surface of the electrodes (see *Discussion*). In fact, as an example of this, if *Fig. 21* is observed carefully, a small hole besides the soldering spot of the cathode can be noticed. The

image also shows rests of the PFA coating that has been stripped previously in order to facilitate the soldering process. Also noticeable is the fact that, as it was previously mentioned, the wires are soldered axially with respect to the electrodes.

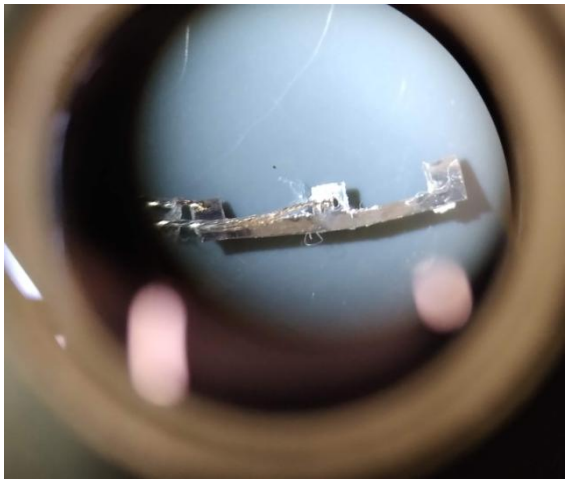

Fig. 21. Stainless steel wires soldered to the electrodes.

The steps that have just been showed with the last figures are shared between all the processes of manufacture tested. Once reached this point, the three mentioned alternatives were tried. The methodology that was more similar to the paper of reference resulted in the cuff electrodes of *Fig. 5* and *Fig. 6* of the *Supporting Information* section. In the first one of these two figures the commented misalignment of the two sheets that compose the cuff can be appreciated. Hence, the cuff of *Fig. 5* has been trimmed to correct that misalignment, reducing the expected dimensions of the cuff. These problems with the manufacturing process were parcially corrected in the second methodology, as it can be appreciated in *Fig. 7* of the *Supporting Information* section, resulted in a cleaner cuff. Nevertheless, due to the problems mentioned in the *Materials and Methods* section, it was the third methodology the one which proved to work best, leading to undamaged electrodes among the sheets and to a more precise process. *Fig. 22* shows how the pre-cut windows fit quite well the electrodes and in *Fig. 23* a global perspective of the cuff can be seen. It has to be taken into account that these electrodes would not be functional, since as it can be appreciated in both images only one wire is connected to them. The other wire came loose during its manipulation for the fabrication of the cuff, which also proves another of the problems that current soldering technique leads to.

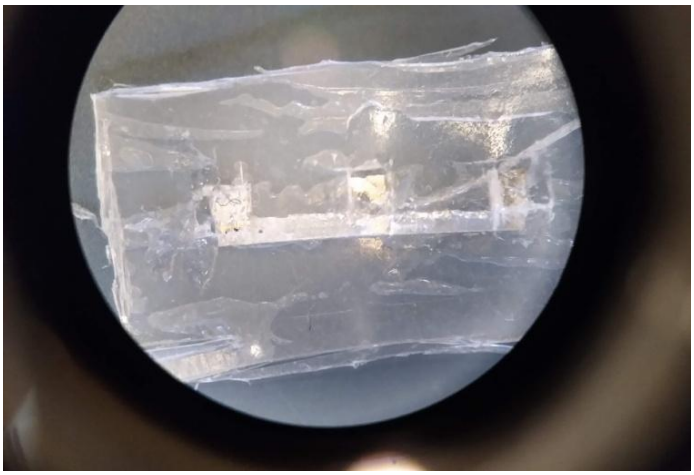

Fig. 22. Cuff electrodes with the windows already opened and the cathode isolated

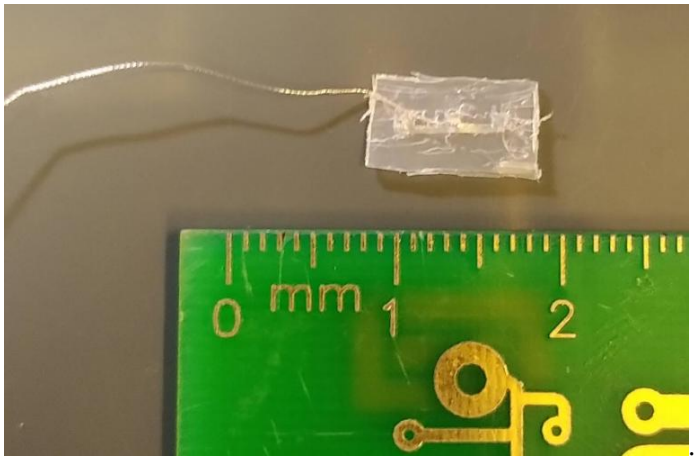

Fig. 23. Global perspective of the fabricated cuff electrodes.

4. DISCUSSION

Regarding the simulations with the PSSI2021SAY, there are two points that completely depend on the choice of the designer of the stimulator: the value of the blocking capacitor used to generate biphasic stimulation and the time that is given to it to discharge. The other parameters, for instance amplitude or frequency of the stimulation, depend on the target of the stimulator (in this case vagus nerve of mice). Thus, the bigger the capacitance of the blocking capacitor is, the more time it needs to fully discharge. The maximum discharge time for a 20Hz stimulation frequency (i.e. 50ms period) is around 45ms so that both phases do not overlap. Otherwise, if the chosen capacitance is too small it produces peaks of current rather than pulses in the cathodic phase, because the voltage at it increases too quickly and the supply voltage of the source is not enough to stabilize that current. Therefore, as it can be noticed, there has to be a balance between achieving the desired shape wave and generating an anodic phase. Another point that has to be considered when working with the simulations of the current source is initialising the voltage at the blocking capacitor at 0V.

Moving on to the simulations of the LT3467, the most remarkable point is the chosen time while it is switched on. Ideally this device should be activated only when the current source is activated, hence when a pulse is going to be delivered. Therefore, it should stay activated during the 500µs of supply that the source needs to produce a

pulse and to work also with a 50ms period. Nevertheless, such a small fraction of time in on state does not allow the converter to output 20V along time and the voltage decays (see *Fig. 24*). This problem is minimized if the converter is switched on during more time than the needed, for instance during 5ms within its 50ms period (*Fig. 25*). However, this clearly implies a waste of current, especially taking into consideration that, as has been showed, the power consumption of the LT3467 is the biggest of all the components of the stimulator. Indeed, knowing the capacity of the chosen CR1025 battery and this current consumption, and neglecting the consumption of the rest of the components, it can be estimated that the LT3467 could be switched on draining current from 3V during about 1 hour and 40 minutes (i.e. 5,976,000ms). Therefore, with the conditions described for *Fig. 25* behaviour, 1,195,200 pulses could be produced. Assuming a 20Hz stimulation frequency and the previously mentioned duty cycle of epilepsy, 600 pulses would be required per cycle. This yields that around 1992 cycles could be delivered taking into consideration only the current consumption of the LT3467.

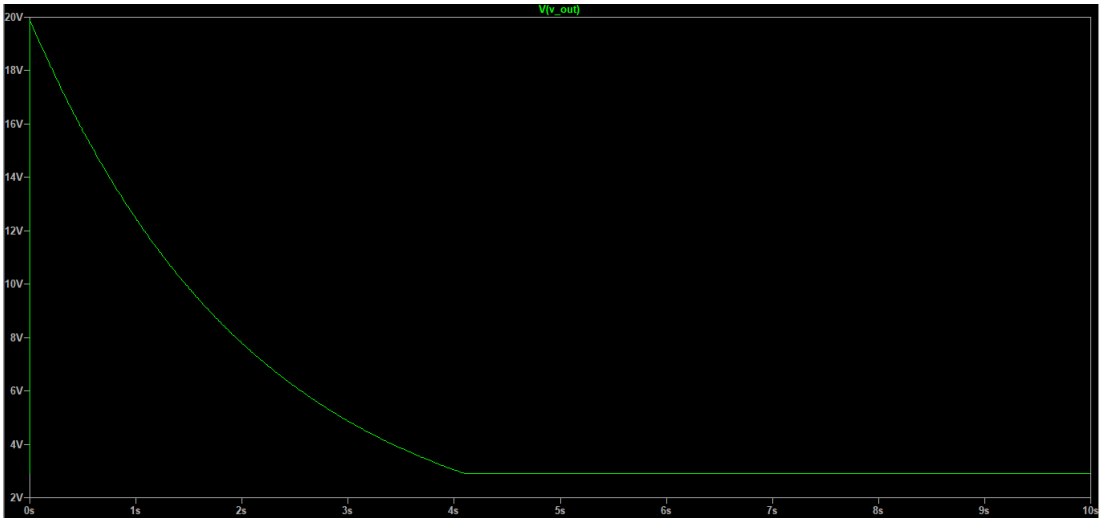

Fig. 24. Output voltage of the LT3467 when being activated under the conditions referred above.

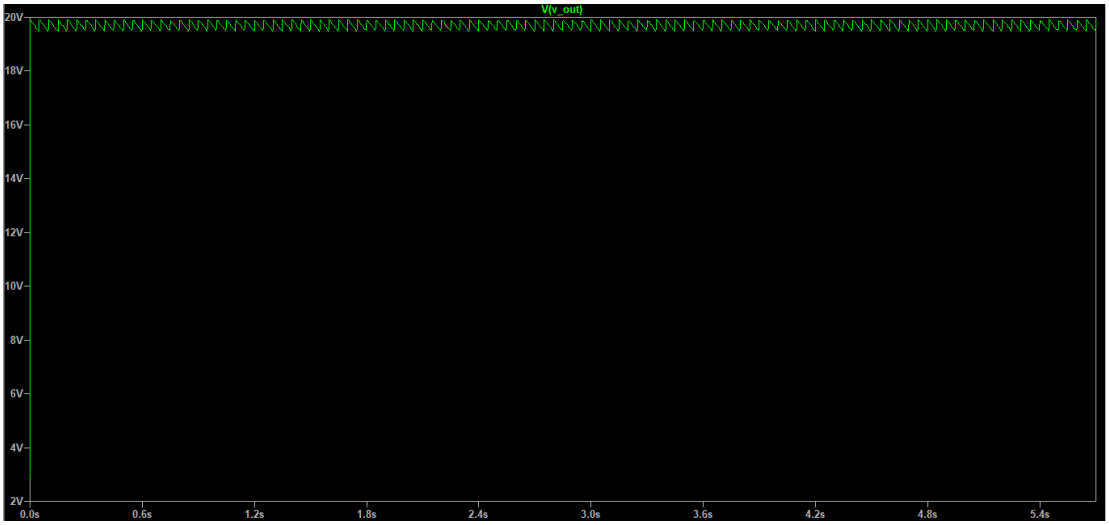

Fig. 25. Output voltage of the LT3467 when being activated under the second conditions referred.

If that time analysis is performed to know how much time the stimulator can be switched off without running out of battery, the consumption of all the components connected to 3V in their off state has to be considered. Therefore, taking into account the theoretical consumption of the microcontroller in its lowest mode (2µA), the consumption of the LT3467 (12µA), the DRV5032 (1µA) and some capacitors (13µA), there is a total basal consumption of 28µA. This yields a survival time for the stimulator of 1071 hours and 25 minutes (i.e. around 44 days and 15 hours).

When it comes to other points related with the design of the stimulator, a case that illustrates pretty well the two big challenges of the work (miniaturization and power consumption) is the one of the photodiode and its comparator. If saving battery was not a priority, the photodiode could be directly connected to 3V instead of being connected to a GPIO pin of the KL03. Hence, the cost of fabrication of the stimulator would decrease, since there would be no need of using a central pin of the MCU and then laser drilling microvias would be avoided. On the other hand, the voltage reference needed to be compared with the output voltage of the photodiode could be created by different ways. Nevertheless most of the options considered do not accomplish the two so-called principles of this work, for instance a voltage divider or an external voltage reference would make the stimulator bulkier and would increase the already-challenging packaging issue. Thus, it is concluded that at the end the most efficient alternative is using the internal *V_REF_OUT* functionality of the KL03.

Finally, regarding manufacture of the electrodes, despite at the end a quite feasible method of fabrication was achieved, the trouble related with the holes that were produced when soldering the electrodes with the laser machine could not be solved. This problem arises due to two circumstances, namely the difference in the type of the used materials (i.e. stainless steel and platinum) and the small dimensions of both of them (especially when it comes to the wire). Since both materials are different they have different melting points. This should not be an issue, since when this happens the one with a higher melting point (the wires in this case) is placed onto the one with a lower melting point (the electrodes in this case). In that way the creation of damages in the structure of the material with a lower melting point should be avoided. Nevertheless, this turns into a trouble when the wire has a diameter of 75 µm and the minimum width of the laser rays for the machine that has been used is 100 µm. This factor, added to the fact that this laser welding machine works completely manually (both processes: calibration and shooting), makes out of the soldering task a really challenging work. Hence, when rays of the beam directly collision with the platinum without passing first through the stainless steel, holes are produced. Therefore, a lot of precision is required to achieve an accurate result. If a lot of time is devoted to calibrate the machine with the materials that are going to be used and many experiments are performed previously to adjust accurately the rays, this problem may be avoided but yet success would not be ensured. Another alternative would be using a spot welder, which is the technology used in L. Foldes et al. [43] for the original process of manufacture.

5. CONCLUSIONS

To sum up, despite some blocks of the stimulator could not be tested (mainly the photodiode and the Hall-effect sensor) and all the control for the performed experiments was done through external devices (e.g. Arduino and voltage source), the obtained results with the evaluation board were mostly successful, which points at a potential viability of the designed vagus nerve stimulator.

On the other hand, it seems clear that in the case of the electrodes the welding technique must be improved, since the wires can break with current methodology. Moreover, the performance of the electrodes could not be tested. Nevertheless, the original methodology of manufacture has been clearly enhanced by making it less bound to damage the electrodes. This can help future students involved in the project by saving both; resources and time.

BIBLIOGRAPHY

[1] Johnson RL, Wilson CG. A review of vagus nerve stimulation as a therapeutic intervention. J Inflamm Res. 2018 May 16;11:203-213. doi: 10.2147/JIR.S163248. PMID: 29844694; PMCID: PMC5961632.
[2] Mollet L, Raedt R, Delbeke J, El Tahry R, Grimonprez A, Dauwe I, DE Herdt V, Meurs A, Wadman W, Boon P, Vonck K. Electrophysiological responses from vagus nerve stimulation in rats. Int J Neural Syst. 2013 Dec;23(6):1350027. doi: 10.1142/S0129065713500275. Epub 2013 Sep 4. PMID: 24156670.
[3] Groves DA, Brown VJ. Vagal nerve stimulation: a review of its applications and potential mechanisms that mediate its clinical effects. Neurosci Biobehav Rev. 2005 May;29(3):493-500. doi: 10.1016/j.neubiorev.2005.01.004. PMID: 15820552.
[4] Ruffoli R, Giorgi FS, Pizzanelli C, Murri L, Paparelli A, Fornai F. The chemical neuroanatomy of vagus nerve stimulation. J Chem Neuroanat. 2011 Dec;42(4):288-96. doi: 10.1016/j.jchemneu.2010.12.002. Epub 2010 Dec 16. PMID: 21167932.
[5] Bonaz B, Picq C, Sinniger V, Mayol JF, Clarençon D. Vagus nerve stimulation: from epilepsy to the cholinergic anti-inflammatory pathway. Neurogastroenterol Motil. 2013 Mar;25(3):208-21. doi: 10.1111/nmo.12076. Epub 2013 Jan 29. PMID: 23360102.
[6] Berthoud HR, Neuhuber WL. Functional and chemical anatomy of the afferent vagal system. Auton Neurosci. 2000 Dec 20;85(1-3):1-17. doi: 10.1016/S1566-0702(00)00215-0. PMID: 11189015.
[7] Browning KN, Travagli RA. Central nervous system control of gastrointestinal motility and secretion and modulation of gastrointestinal functions. Compr Physiol. 2014 Oct;4(4):1339-68. doi: 10.1002/cphy.c130055. PMID: 25428846; PMCID: PMC4858318.
[8] Tracey KJ. The inflammatory reflex. Nature. 2002 Dec 19-26;420(6917):853-9. doi: 10.1038/nature01321. PMID: 12490958.
[9] Spuck S, Nowak G, Renneberg A, Tronnier V, Sperner J. Right-sided vagus nerve stimulation in humans: an effective therapy? Epilepsy Res. 2008 Dec;82(2-3):232-4. doi: 10.1016/j.eplepsyres.2008.08.003. Epub 2008 Sep 18. PMID: 18801642.
[10] Bajbouj M, Merkl A, Schlaepfer TE, Frick C, Zobel A, Maier W, O'Keane V, Corcoran C, Adolfsson R, Trimble M, Rau H, Hoff HJ, Padberg F, Müller-Siecheneder F, Audenaert K, van den Abbeele D, Matthews K, Christmas D, Eljamel S, Heuser I. Two-year outcome of vagus nerve stimulation in treatment-resistant depression. J Clin Psychopharmacol. 2010 Jun;30(3):273-81. doi: 10.1097/JCP.0b013e3181db8831. PMID: 20473062.
[11] Val-Laillet D, Biraben A, Randuineau G, Malbert CH. Chronic vagus nerve stimulation decreased weight gain, food consumption and sweet craving in adult obese minipigs. Appetite. 2010 Oct;55(2):245-52. doi: 10.1016/j.appet.2010.06.008. Epub 2010 Jun 19. PMID: 20600417.
[12] Zhang Y, Popovic ZB, Bibevski S, Fakhry I, Sica DA, Van Wagoner DR, Mazgalev TN. Chronic vagus nerve stimulation improves autonomic control and attenuates systemic inflammation and heart failure progression in a canine high-rate pacing model. Circ Heart Fail. 2009 Nov;2(6):692-9. doi: 10.1161/CIRCHEARTFAILURE.109.873968. Epub 2009 Sep 22. PMID: 19919995.
[13] Meyers EE, Kronemberger A, Lira V, Rahmouni K, Stauss HM. Contrasting effects of afferent and efferent vagal nerve stimulation on insulin secretion and blood glucose regulation. Physiol Rep. 2016 Feb;4(4):e12718. doi: 10.14814/phy2.12718. PMID: 26884478; PMCID: PMC4759047.

[14] Elliott RE, Rodgers SD, Bassani L, Morsi A, Geller EB, Carlson C, Devinsky O, Doyle WK. Vagus nerve stimulation for children with treatment-resistant epilepsy: a consecutive series of 141 cases. J Neurosurg Pediatr. 2011 May;7(5):491-500. doi: 10.3171/2011.2.PEDS10505. PMID: 21529189.
[15] Ben-Menachem E, Revesz D, Simon BJ, Silberstein S. Surgically implanted and non-invasive vagus nerve stimulation: a review of efficacy, safety and tolerability. Eur J Neurol. 2015 Sep;22(9):1260-8. doi: 10.1111/ene.12629. Epub 2015 Jan 23. PMID: 25614179; PMCID: PMC5024045.
[16] Heck, C., Helmers, S. L., and DeGiorgio, C. M. (2002). Vagus nerve stimulation therapy, epilepsy, and device parameters: scientific basis and recommendations for use. Neurology 59(6 Suppl. 4), S31–S37.
[17] Merrill DR, Bikson M, Jefferys JG. Electrical stimulation of excitable tissue: design of efficacious and safe protocols. J Neurosci Methods. 2005 Feb 15;141(2):171-98. doi: 10.1016/j.jneumeth.2004.10.020. PMID: 15661300.
[18] Mortimer, John & Bhadra, Narendra. (2018). Fundamentals of Electrical Stimulation. 10.1016/B978-0-12-805353-9.00006-1.
[19] Howland RH. Vagus Nerve Stimulation. Curr Behav Neurosci Rep. 2014 Jun;1(2):64-73. doi: 10.1007/s40473-014-0010-5. PMID: 24834378; PMCID: PMC4017164.
[20] Hong GS, Zillekens A, Schneiker B, Pantelis D, de Jonge WJ, Schaefer N, Kalff JC, Wehner S. Non-invasive transcutaneous auricular vagus nerve stimulation prevents postoperative ileus and endotoxemia in mice. Neurogastroenterol Motil. 2019 Mar;31(3):e13501. doi: 10.1111/nmo.13501. Epub 2018 Nov 8. PMID: 30406957.
[21] Noller CM, Levine YA, Urakov TM, Aronson JP, Nash MS. Vagus Nerve Stimulation in Rodent Models: An Overview of Technical Considerations. Front Neurosci. 2019 Sep 4;13:911. doi: 10.3389/fnins.2019.00911. PMID: 31551679; PMCID: PMC6738225.
[22] Krahl SE, Senanayake SS, Handforth A. Destruction of peripheral C-fibers does not alter subsequent vagus nerve stimulation-induced seizure suppression in rats. Epilepsia. 2001 May;42(5):586-9. doi: 10.1046/j.1528-1157.2001.09700.x. PMID: 11380564.
[23] Agnew WF, McCreery DB, Yuen TG, Bullara LA. Evolution and resolution of stimulation-induced axonal injury in peripheral nerve. Muscle Nerve. 1999 Oct;22(10):1393-402. doi: 10.1002/(sici)1097-4598(199910)22:10<1393::aid-mus9>3.0.co;2-e. PMID: 10487906.
[24] Agnew WF, McCreery DB. Considerations for safety with chronically implanted nerve electrodes. Epilepsia. 1990;31 Suppl 2:S27-32. doi: 10.1111/j.1528-1157.1990.tb05845.x. PMID: 2226363.
[25] Zabara J. Inhibition of experimental seizures in canines by repetitive vagal stimulation. Epilepsia. 1992 Nov-Dec;33(6):1005-12. doi: 10.1111/j.1528-1157.1992.tb01751.x. PMID: 1464256.
[26] Yao G, Kang L, Li J, Long Y, Wei H, Ferreira CA, Jeffery JJ, Lin Y, Cai W, Wang X. Effective weight control via an implanted self-powered vagus nerve stimulation device. Nat Commun. 2018 Dec 17;9(1):5349. doi: 10.1038/s41467-018-07764-z. PMID: 30559435; PMCID: PMC6297229.
[27] Lee B, Koripalli MK, Jia Y, Acosta J, Sendi MSE, Choi Y, Ghovanloo M. An Implantable Peripheral Nerve Recording and Stimulation System for Experiments on Freely Moving Animal Subjects. Sci Rep. 2018 Apr 17;8(1):6115. doi: 10.1038/s41598-018-24465-1. PMID: 29666407; PMCID: PMC5904113.

[28] Rui B, Guo S, Zeng B, Wang J, Chen X. An implantable electrical stimulator used for peripheral nerve rehabilitation in rats. Exp Ther Med. 2013 Jul;6(1):22-28. doi: 10.3892/etm.2013.1110. Epub 2013 May 13. PMID: 23935712; PMCID: PMC3735806.
[29] El Tahry R, Raedt R, Mollet L, De Herdt V, Wyckhuys T, Van Dycke A, Meurs A, Dewaele F, Van Roost D, Doguet P, Delbeke J, Wadman W, Vonck K, Boon P. A novel implantable vagus nerve stimulation system (ADNS-300) for combined stimulation and recording of the vagus nerve: pilot trial at Ghent University Hospital. Epilepsy Res. 2010 Dec;92(2-3):231-9. doi: 10.1016/j.eplepsyres.2010.10.007. Epub 2010 Nov 10. Erratum in: Epilepsy Res. 2012 Nov;102(1-2):131-2. Wyckuys, Tine [corrected to Wyckhuys, Tine]. PMID: 21071177.
[30] Bard AJ, Faulkner LR. Electrochemical methods. New York: Wiley; 1980 p. 19 and 102 [Chapters 1.3.3, 2, 3.5 and 9.1.3].
[31] Halliwell B. Reactive oxygen species and the central nervous system. J. Neurochem 1992;59(5):1609–23.
[32] Hemnani T, Parihar MS. Reactive oxygen species and oxidative DNA damage. Indian J Physiol Pharmacol 1998;42(4):440–52.
[33] Kumsa, D., Hudak, E.M., Montague, F.W., Kelley, S.C., Untereker, D.F., Hahn, B.P., Condit, C., Cholette, M., Lee, H., Bardot, D., Takmakov, P., 2016b. Electrical neurostimulation with imbalanced waveform mitigates dissolution of platinum electrodes. J. Neural Eng. 13 (5).
[34] Jia Y, Gong Y, Weber A, Li W, Ghovanloo M. A mm-Sized Free-Floating Wireless Implantable Opto-Electro Stimulation Device. Micromachines (Basel). 2020 Jun 25;11(6):621. doi: 10.3390/mi11060621. PMID: 32630557; PMCID: PMC7345121.
[35] Hoffer, Joaquin & Kallesoe, Klaus. (1999). NERVE CUFF ELECTRODES FOR PROSTHETIC AND RESEARCH APPLICATIONS.
[36] Hoffer, Joaquin & Kallesoe, Klaus. (2000). How to Use Nerve Cuffs to Stimulate, Record or Modulate Neural Activity. 10.1201/9781420039054.ch5.
[37] Stauss HM. Differential hemodynamic and respiratory responses to right and left cervical vagal nerve stimulation in rats. Physiol Rep. 2017 Apr;5(7):e13244. doi: 10.14814/phy2.13244. PMID: 28400500; PMCID: PMC5392529.
[38] Chapleau MW, Rotella DL, Reho JJ, Rahmouni K, Stauss HM. Chronic vagal nerve stimulation prevents high-salt diet-induced endothelial dysfunction and aortic stiffening in stroke-prone spontaneously hypertensive rats. Am J Physiol Heart Circ Physiol. 2016 Jul 1;311(1):H276-85. doi: 10.1152/ajpheart.00043.2016. Epub 2016 May 20. PMID: 27208157; PMCID: PMC4967207.
[39] F. Kölbl et al., "An Embedded Deep Brain Stimulator for Biphasic Chronic Experiments in Freely Moving Rodents," in IEEE Transactions on Biomedical Circuits and Systems, vol. 10, no. 1, pp. 72-84, Feb. 2016, doi: 10.1109/TBCAS.2014.2368788.
[40] Adams SD, Bennet KE, Tye SJ, Berk M, Kouzani AZ. Development of a miniature device for emerging deep brain stimulation paradigms. PLoS One. 2019 Feb 21;14(2):e0212554. doi: 10.1371/journal.pone.0212554. PMID: 30789946; PMCID: PMC6383994.
[41] Ewing SG, Porr B, Riddell J, Winter C, Grace AA. SaBer DBS: a fully programmable, rechargeable, bilateral, charge-balanced preclinical microstimulator for long-term neural stimulation. J Neurosci Methods. 2013 Mar 15;213(2):228-35. doi: 10.1016/j.jneumeth.2012.12.008. Epub 2013 Jan 7. PMID: 23305773; PMCID: PMC3574185.
[42] Yaghouby, Farid & Shafer, Benjamin & Vasudevan, Srikanth. (2019). A rodent model for long-term vagus nerve stimulation experiments. Bioelectronics in Medicine. 2. 10.2217/bem-2019-0016.

[43] Foldes EL, Ackermann DM, Bhadra N, Kilgore KL, Bhadra N. Design, fabrication and evaluation of a conforming circumpolar peripheral nerve cuff electrode for acute experimental use. J Neurosci Methods. 2011 Mar 15;196(1):31-7. doi: 10.1016/j.jneumeth.2010.12.020. Epub 2010 Dec 25. PMID: 21187115; PMCID: PMC3042051.
[44] Naples GG, Mortimer JT, Scheiner A, Sweeney JD. A spiral nerve cuff electrode for peripheral nerve stimulation. IEEE Trans Biomed Eng. 1988 Nov;35(11):905-16. doi: 10.1109/10.8670. PMID: 3198136.
[45] J.T. Mortimer. Applied Neural Control. Department of Biomedical Engineering, Case Western Reserve University online resources: link.

SUPPORTING INFORMATION

Note: since the resolution of the EAGLE sketches is low in these images, they are attached with a higher quality at the end of this section (in the same order).

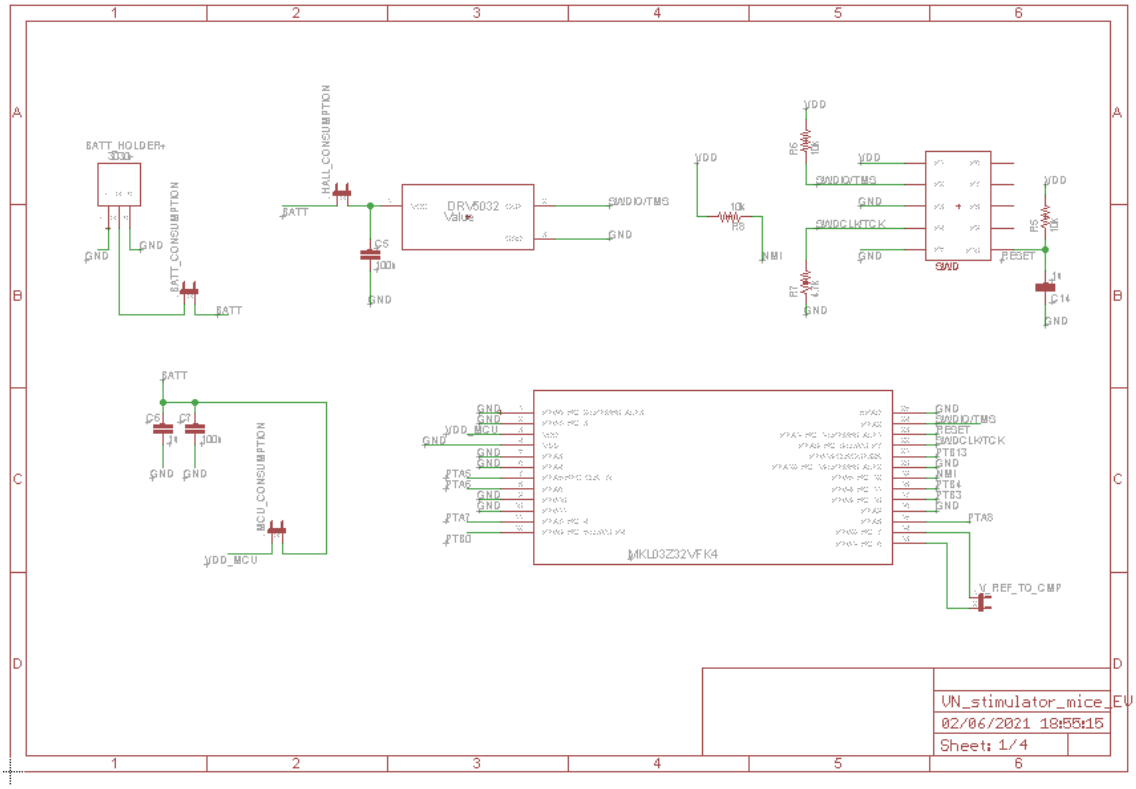

Fig. 1. Page 1 of the schematic of the evaluation board of the vagus nerve stimulator.

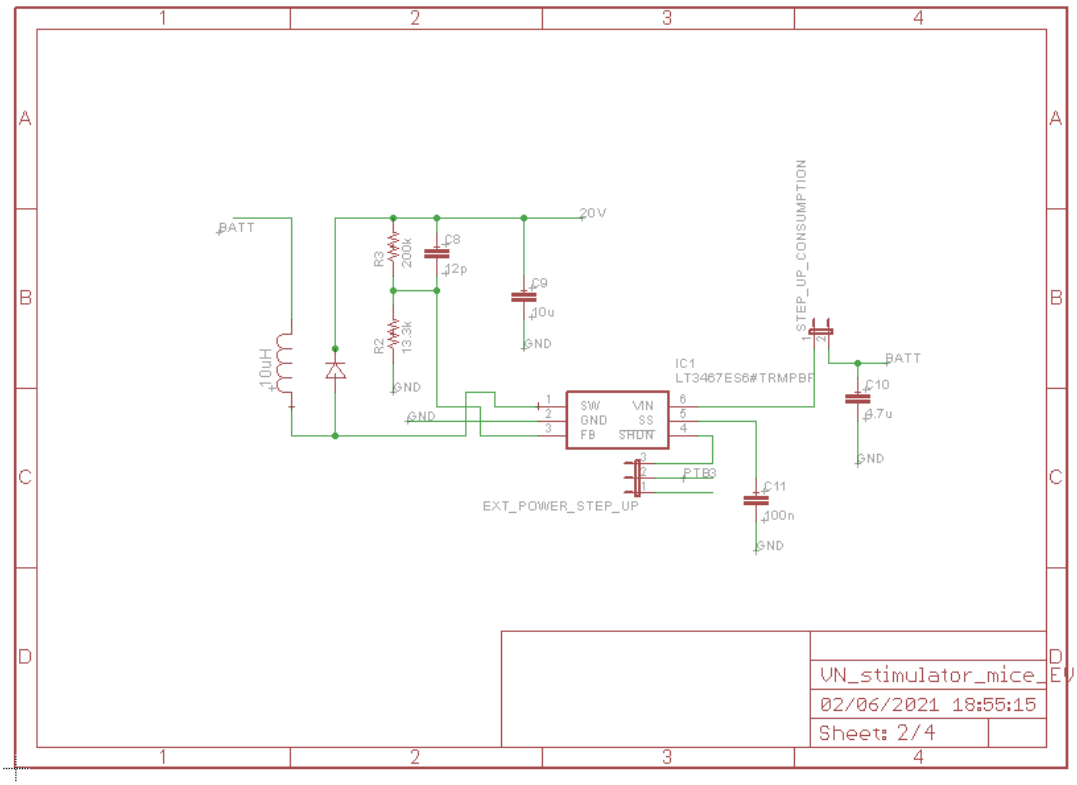

Fig. 2. Page 2 of the schematic of the evaluation board of the vagus nerve stimulator.

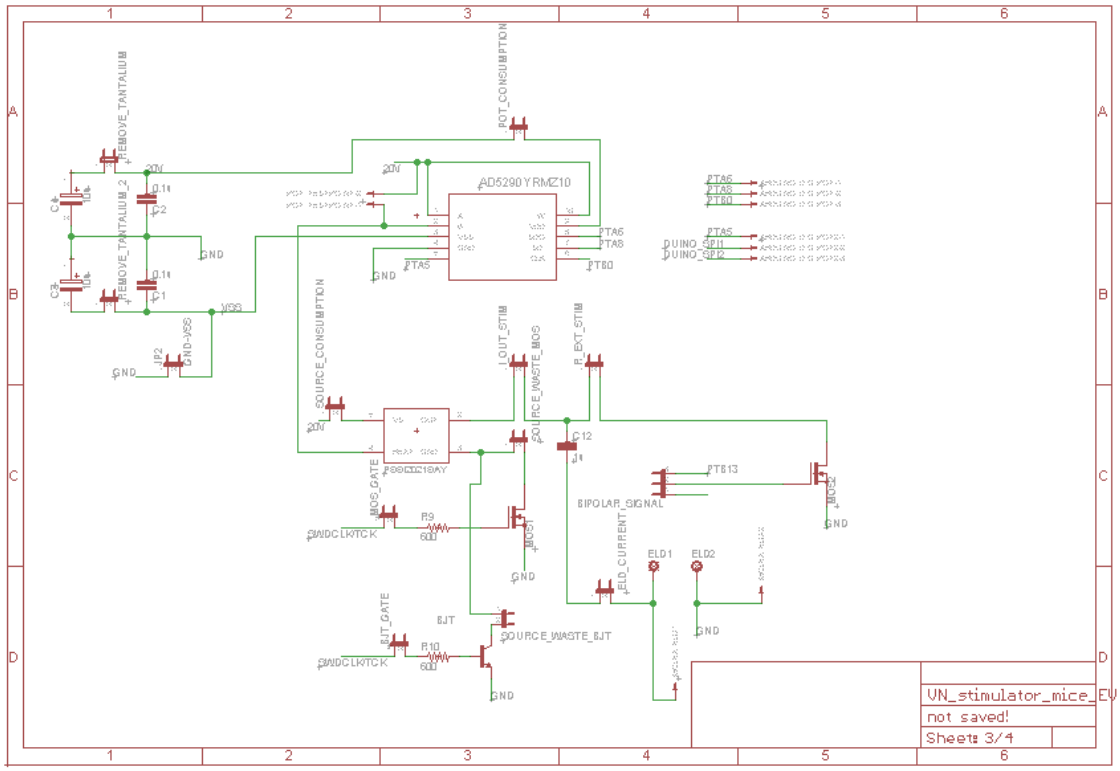

Fig. 3. Page 3 of the schematic of the evaluation board of the vagus nerve stimulator.

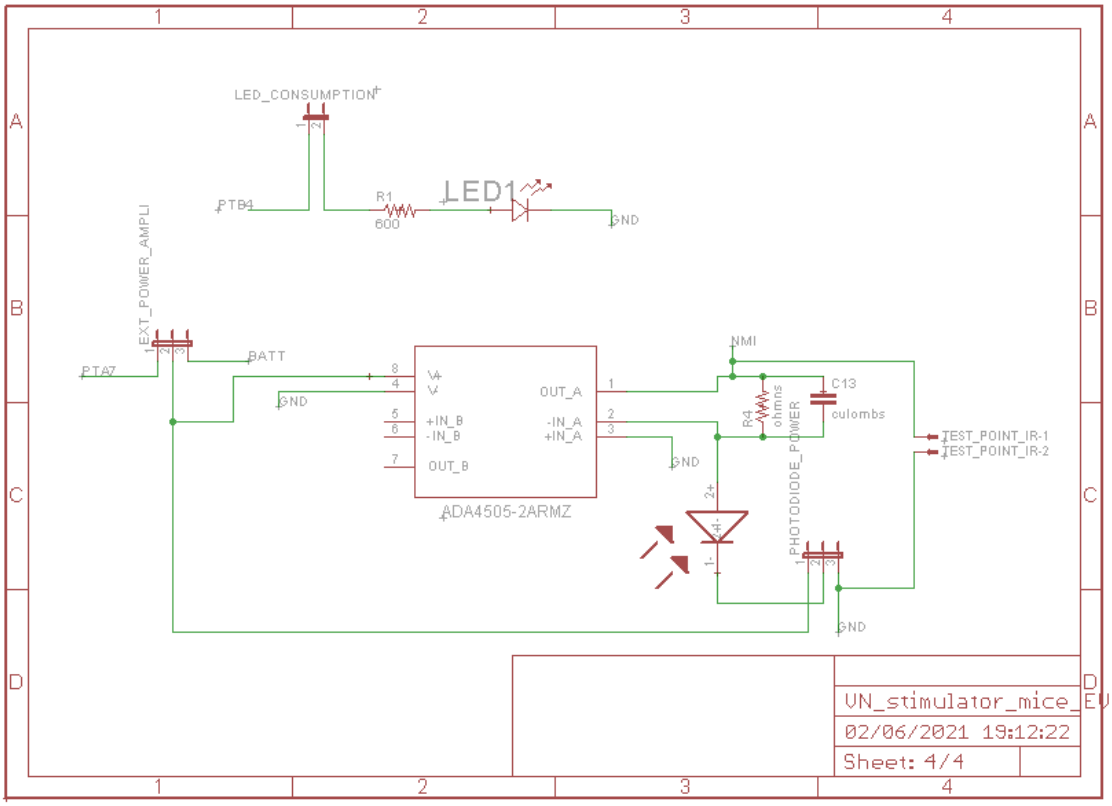

Fig. 4. Page 4 of the schematic of the evaluation board of the vagus nerve stimulator.

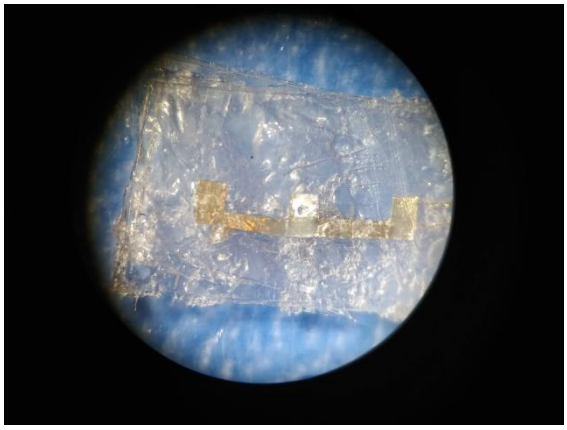

Fig. 5. Cuff that resulted from the first methodology of fabrication tried.

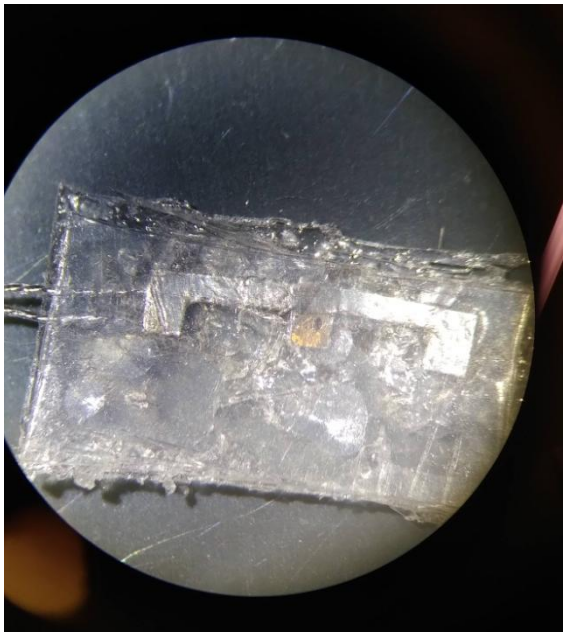

Fig. 6. Cuff of the previous figure trimmed to correct the misalignments.

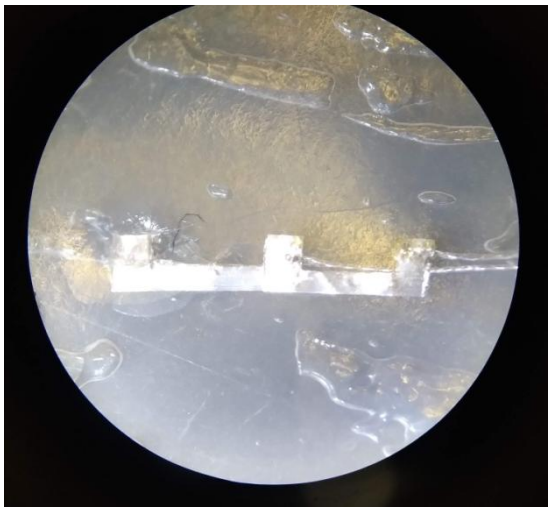

Fig. 7. Sandwich that resulted from the second methodology of fabrication tried.

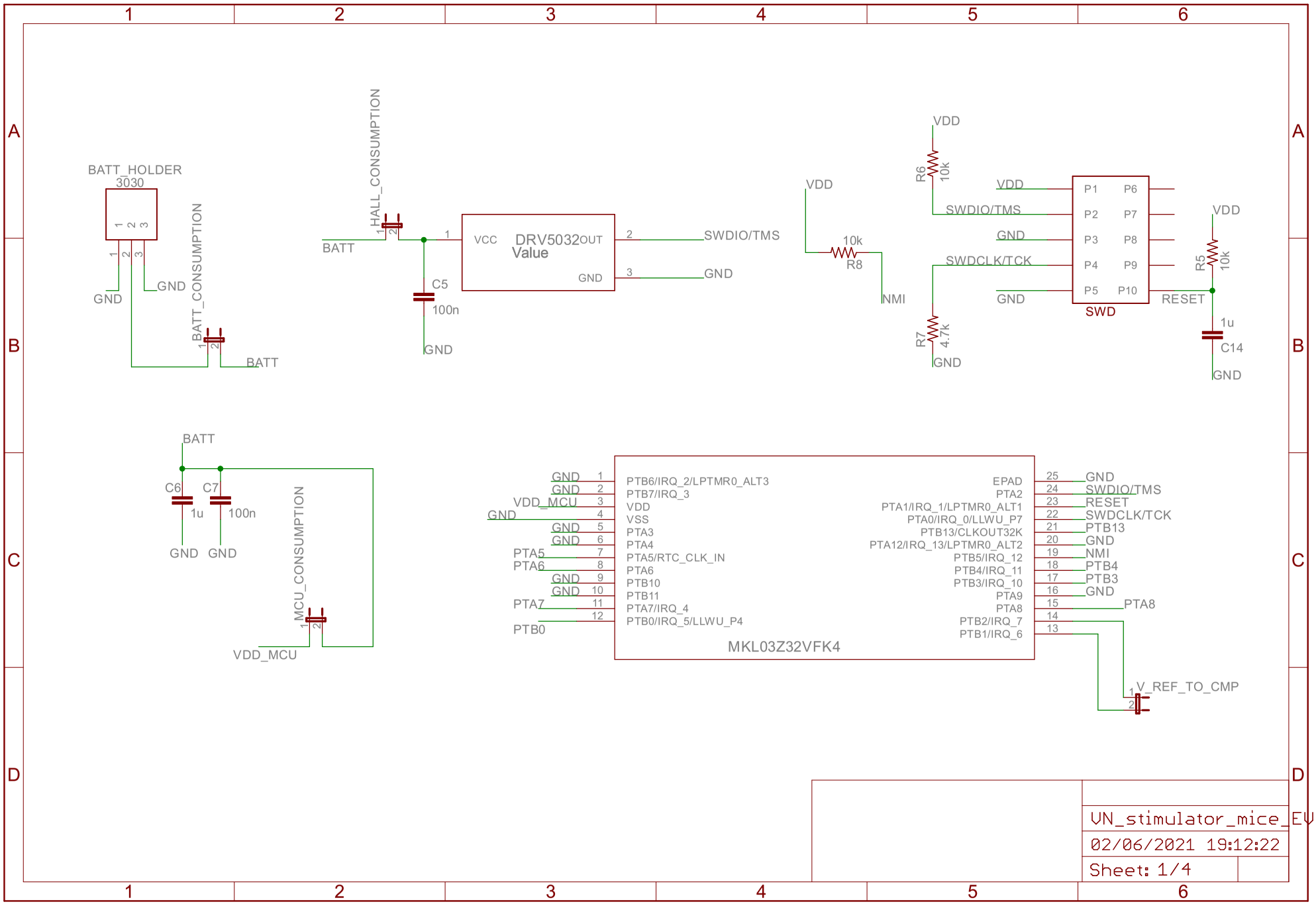
BATT_HOLDER
3030
GND
GND
BATT_CONSUMPTION
BATT
HALL_CONSUMPTION
BATT
VCC
DRV5032OUT
Value
GND
SWDIO/TMS
GND
C5
100n
GND
VDD
10k
R8
NMI
VDD
R6
10k
VDD
SWDIO/TMS
GND
SWDCLK/TCK
GND
P1
P2
P3
P4
P5
P6
P7
P8
P9
P10
SWD
VDD
R5
10k
RESET
1u
C14
GND
R7
4.7k
GND
BATT
C6
1u
C7
100n
GND
GND
MCU_CONSUMPTION
VDD_MCU
GND
GND
VDD_MCU
GND
GND
PTA5
PTA6
GND
GND
PTA7
PTB0
PTB6/IRQ_2/LPTMR0_ALT3
PTB7/IRQ_3
VDD
VSS
PTA3
PTA4
PTA5/RTC_CLK_IN
PTA6
PTB10
PTB11
PTA7/IRQ_4
PTB0/IRQ_5/LLWU_P4
MKL03Z32VFK4
EPAD
PTA2
PTA1/IRQ_1/LPTMR0_ALT1
PTA0/IRQ_0/LLWU_P7
PTB13/CLKOUT32K
PTA12/IRQ_13/LPTMR0_ALT2
PTB5/IRQ_12
PTB4/IRQ_11
PTB3/IRQ_10
PTA9
PTA8
PTB2/IRQ_7
PTB1/IRQ_6
GND
SWDIO/TMS
RESET
SWDCLK/TCK
PTB13
GND
NMI
PTB4
PTB3
GND
PTA8
V_REF_TO_CMP
UN_stimulator_mice_EU
02/06/2021 19:12:22
Sheet: 1/4

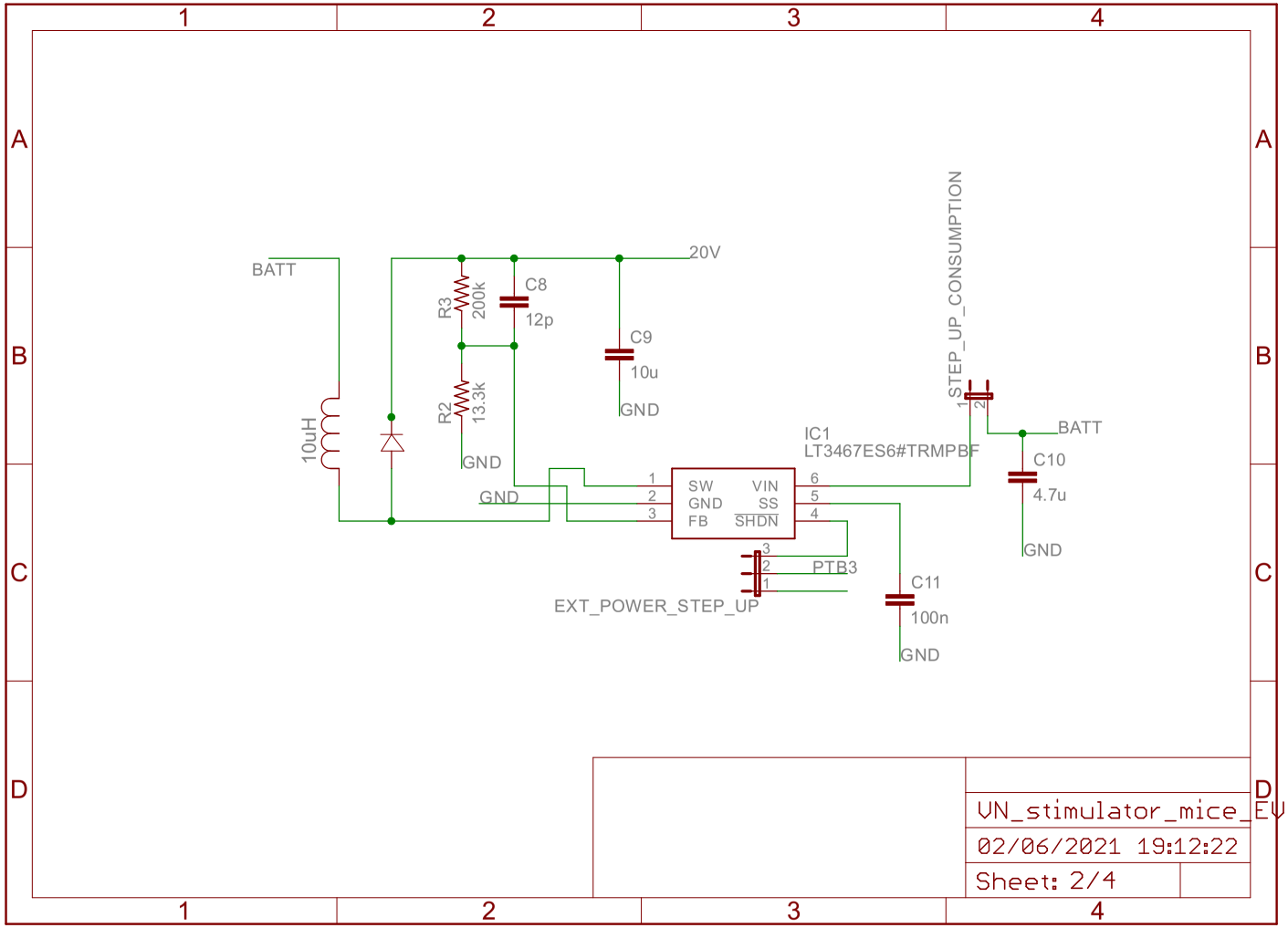
1
2
3
4
A
B
C
D
BATT
10uH
R3
200k
C8
12p
R2
13.3k
GND
20V
C9
10u
GND
STEP_UP_CONSUMPTION
IC1
LT3467ES6#TRMPBF
SW
GND
FB
VIN
SS
SHDN
GND
BATT
C10
4.7u
GND
PTB3
EXT_POWER_STEP_UP
C11
100n
GND
VN_stimulator_mice_EU
02/06/2021 19:12:22
Sheet: 2/4

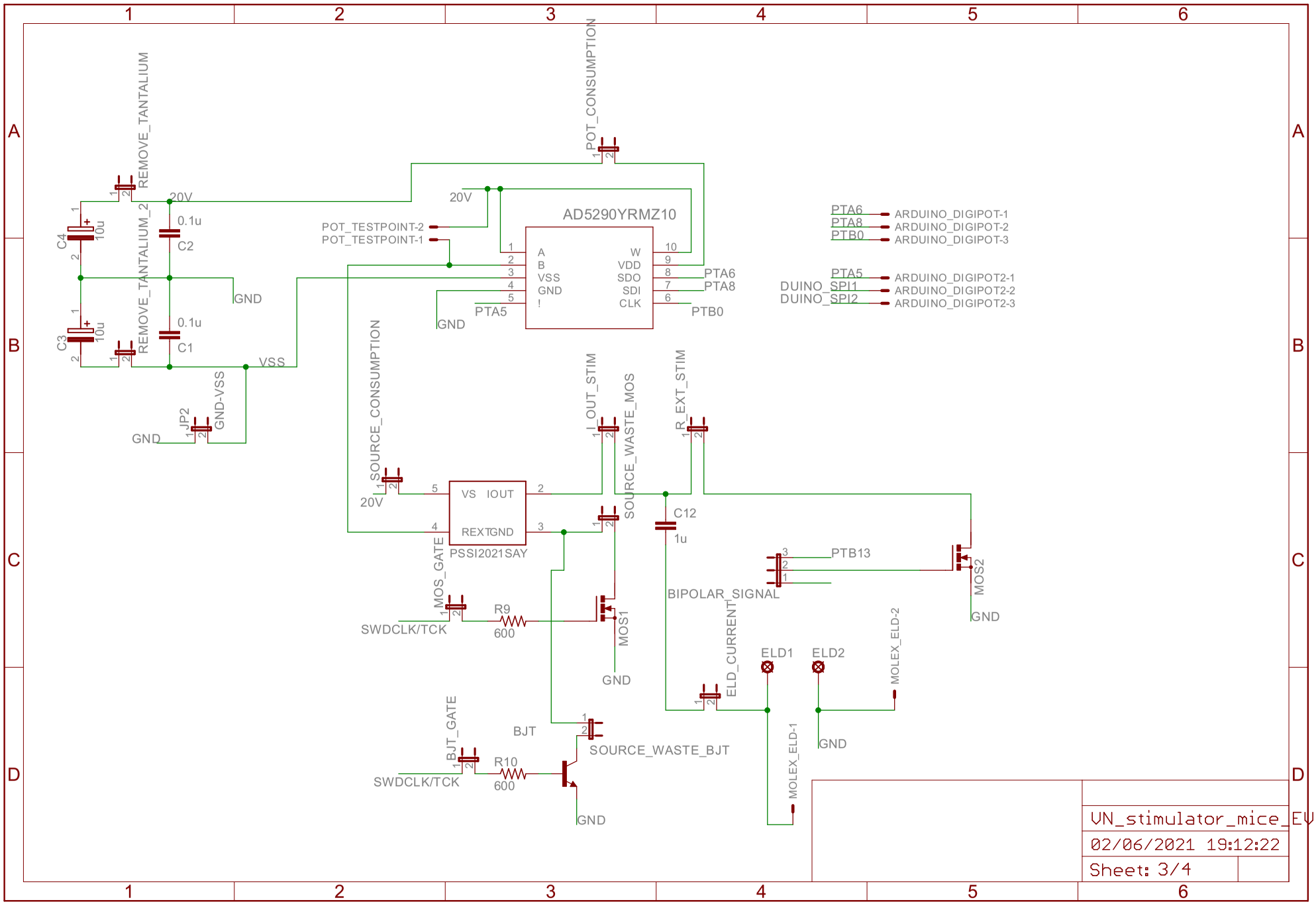
REMOVE_TANTALIUM
POT_CONSUMPTION
20V
0.1u
C2
C4
10u
REMOVE_TANTALIUM_2
GND
C3
C1
VSS
GND-VSS
JP2
GND
POT_TESTPOINT-2
POT_TESTPOINT-1
AD5290YRMZ10
A
B
VSS
GND
!
W
VDD
SDO
SDI
CLK
PTA6
PTA8
PTB0
PTA5
PTA6 ARDUINO_DIGIPOT-1
PTA8 ARDUINO_DIGIPOT-2
PTB0 ARDUINO_DIGIPOT-3
PTA5 ARDUINO_DIGIPOT2-1
DUINO_SPI1 ARDUINO_DIGIPOT2-2
DUINO_SPI2 ARDUINO_DIGIPOT2-3
SOURCE_CONSUMPTION
I_OUT_STIM
SOURCE_WASTE_MOS
R_EXT_STIM
VS IOUT
REXTGND
PSSI2021SAY
C12
1u
MOS_GATE
R9
600
SWDCLK/TCK
MOS1
PTB13
MOS2
BIPOLAR_SIGNAL
ELD_CURRENT
ELD1
ELD2
MOLEX_ELD-2
BJT_GATE
BJT
R10
SOURCE_WASTE_BJT
MOLEX_ELD-1
UN_stimulator_mice_EU
02/06/2021 19:12:22
Sheet: 3/4

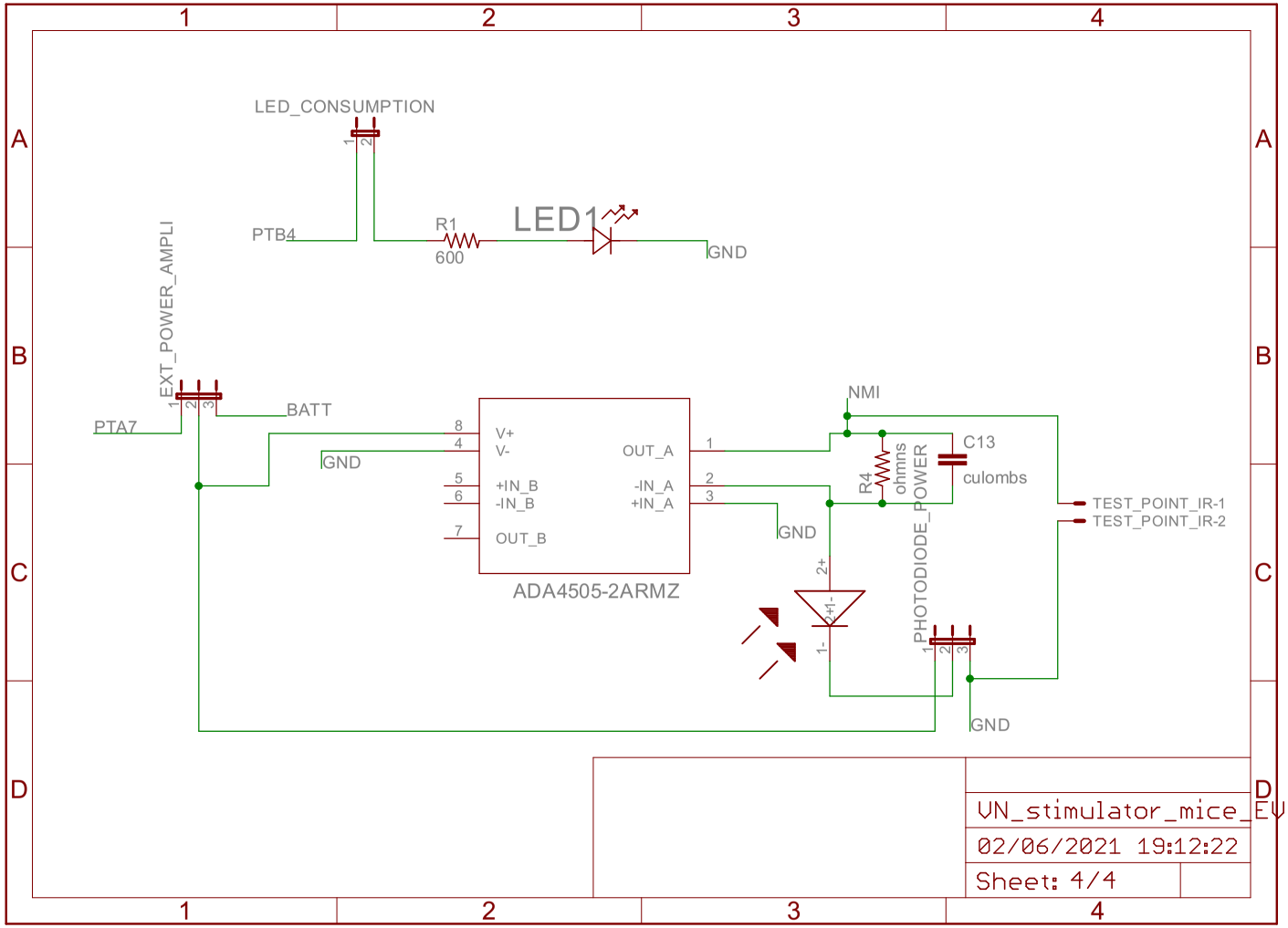
1
2
3
4
A
B
C
D
LED_CONSUMPTION
PTB4
R1
600
LED1
GND
EXT_POWER_AMPLI
PTA7
BATT
GND
V+
V-
OUT_A
+IN_B
-IN_B
OUT_B
-IN_A
+IN_A
ADA4505-2ARMZ
NMI
R4
ohms
C13
culombs
PHOTODIODE_POWER
GND
TEST_POINT_IR-1
TEST_POINT_IR-2
GND
VN_stimulator_mice_EU
02/06/2021 19:12:22
Sheet: 4/4